HHS Public Access

Author manuscript

Sci Transl Med. Author manuscript; available in PMC 2021 September 03.

Published in final edited form as:

Sci Transl Med. 2021 March 03; 13(583): . doi:10.1126/scitranslmed.abb6731.

Dual role of endothelial *Myct1* in tumor angiogenesis and tumor immunity

Ashraf Ul Kabir[1,2], **Madhav Subramanian**[1], **Dong Hun Lee**[3], **Xiaoli Wang**[1], **Karen Krchma**[1], **Jun Wu**[1], **Teri Naismith**[4], **Carmen M. Halabi**[5], **Ju Young Kim**[3], **Fadi E. Pulous**[3], **Brian G. Petrich**[3], **Suhyun Kim**[6], **Hae-Chul Park**[6], **Phyllis I. Hanson**[7], **Hua Pan**[8], **Samuel A. Wickline**[8], **Daved H. Fremont**[1], **Changwon Park**[3,9,*], **Kyunghee Choi**[1,2,10,*]

[1]Department of Pathology and Immunology, Washington University School of Medicine, St. Louis, MO 63110-1093, USA

[2]Molecular and Cell Biology Program, Washington University School of Medicine, St. Louis, MO 63110-1093, USA

[3]Department of Pediatrics, Emory University School of Medicine, Atlanta, GA 30322, USA

[4]Department of Cell Biology and Physiology, Washington University School of Medicine, St. Louis, MO 63110-1093, USA

[5]Department of Pediatrics, Washington University School of Medicine, St. Louis, MO 63110-1093, USA

[6]Department of Biomedical Sciences, College of Medicine, Korea University, Ansan 15335, Republic of Korea

[7]Department of Biological Chemistry, University of Michigan Medical School, Ann Arbor, MI 48109-5624, USA

[8]Health Heart Institute, Morsani College of Medicine, University of South Florida, Tampa, FL 33612, USA

[*]Corresponding Authors, Dr. Changwon Park, Tel: +13186758856, FAX: +1 (318)675-6005, cpar13@lsuhsc.edu mailto:, 1501 Kings Hwy, Shreveport, LA 71103, USA, Dr. Kyunghee Choi, Tel: +1 3143628716, FAX: +1 314-747-0809, kchoi@wustl.edu, Campus Box 8118, 660 S. Euclid Ave. St. Louis, MO, 63110-1093, USA.

Author contributions: A.U.K., C.P., and K.C. conceived and designed experiments and wrote the paper. A.U.K. performed the experiments and analyzed the data. M.S. analyzed the human cancer patient datasets from TCGA database and the mice tumor-EC RNA sequencing datasets. D.H.L. performed the Chip-qPCR and luciferase assays. X.W. and D.H.F helped to design and generate the *Myct1* overexpression plasmids, and the FACS experiment with the *Myct1* overexpressing cells. K.K and J.W. helped with *Myct1* KO and bone-marrow chimeric mice development. M.S., D.H.L., J.Y.K., F.P., and B.P. helped with the in vitro assessment of angiogenic functionalities of endothelial cells. S.K. and H.C.P. performed the zebrafish experiments. T.N. and P.I.H helped with the immunocytochemistry experiments for observing MYCT1 cellular localization. C.M.H helped to measure blood pressure and performed compliance studies. H.P. and S.A.W. generated the peptide for nanoparticle development. K.C. provided overall supervision and coordinated all the experimental activities.

Competing interests: Samuel A. Wickline has Equity in Trasir Therapeutics, Inc. Ashraf Ul Kabir and Kyunghee Choi have a patent pending relating to this work (Application Number: 63/093,595; Title: COMPOSITIONS AND METHODS FOR MODULATING MYCT1). All other authors declare that they have no competing interests.

Data and materials availability: All data associated with this study are available in the main text or the supplementary materials. RNA sequencing data is available as GSE157879 and GSE146819. Global *Myct1* knockout mice and Cdh5-cre *Myct1* knockout mice can be provided to academic researchers via an MTA upon request to Kyunghee Choi and Changwon Park, respectively.

[9]Department of Molecular & Cellular Physiology, Louisiana State University Health Science Center, Shreveport, LA 71103, USA

[10]Graduate School of Biotechnology, Kyung Hee University, Yong In 17104, Korea

Abstract

The crosstalk between angiogenesis and immunity within the tumor microenvironment (TME) is critical for tumor prognosis. While pro-angiogenic and immunosuppressive TME promote tumor growth, anti-angiogenic and immune stimulatory TME inhibit tumor progression. Therefore, there is a great interest in achieving vascular normalization to improve drug delivery and enhance anti-tumor immunity. However, anti-vascular endothelial growth factor (VEGF) mechanisms to normalize tumor vessels have offered limited therapeutic efficacies for cancer patients. Herein, we report that *Myct1*, a direct target of ETV2, was nearly exclusively expressed in endothelial cells. In preclinical mouse tumor models, *Myct1* deficiency reduced angiogenesis, enhanced high endothelial venule formation, and promoted an anti-tumor immune environment, leading to restricted tumor progression in *Myct1* knockout mice. Analysis of The Cancer Genome Atlas (TCGA) datasets revealed a significant ($p<0.05$) correlation between *MYCT1* expression, angiogenesis, and anti-tumor immunity in human cancers, as suggested by the decreased FOXP3 expression and increased anti-tumor macrophages in patients with low *MYCT1* expression. Mechanistically, MYCT1 interacted with tight junction protein Zona Occludens 1 and regulated Rho GTPase-mediated actin cytoskeleton dynamics, thereby promoting endothelial motility in the angiogenic environment. *Myct1*-deficient endothelial cells facilitated trans-endothelial migration of cytotoxic T lymphocytes and polarization of M1 macrophages. *Myct1* targeting combined with anti-PD1 treatment significantly *($p<0.05$)* increased complete tumor regression and long-term survival in anti-PD1-responsive and -refractory tumor models in mice. Our data collectively support a critical role for *Myct1* in controlling tumor angiogenesis and reprogramming tumor immunity. *Myct1*-targeted vascular control, in combination with immunotherapy, may become an exciting therapeutic strategy.

One-sentence summary:

Myct1 inhibition controls tumor angiogenesis, remodels tumor immunity, and improves immunotherapy outcomes in mouse tumor models.

Introduction

Tumor vessels are irregular, tortuous, and leaky. These malfunctioning vessels lead to a hypoxic environment where tumors thrive and eventually metastasize to secondary sites. Following the initial report on the vasculature-dependent nature of solid tumor progression 50 years ago (1), the notion of preventing new vessel formation as a way to treat cancers generated substantial interest. Extensive research has identified several critical pro-angiogenic factors, including vascular endothelial growth factors (VEGFs) and fibroblast growth factors, as potential targets for anti-angiogenic therapies (2, 3). However, despite impressive potential shown in preclinical studies, anti-angiogenic strategies like anti-VEGF treatment generated only modest clinical outcomes in cancer patients, possibly due to temporary vascular normalization, angiogenic adaptive responses, and/or acquired resistance

by the tumor (4, 5). Pro-angiogenic factors like VEGFs are also required for physiological vascular maintenance, contributing to the related toxicities and poor clinical outcomes of anti-VEGF therapies (6–8). As such, new targets are required to develop anti-angiogenic approaches that may empower cancer management.

Immunotherapies such as immune checkpoint blockers and adoptive immune cell transfer have revolutionized the field of oncotherapy by enabling the regression and long-term control of previously incurable and aggressive tumors. However, they fail to produce clinical benefits in 50%−80% of treated patients (9), suggesting that further studies focusing on the functional crosstalk between different immunotherapeutic approaches and the constituents of the tumor microenvironment are needed. Accumulating data show that the abnormal nature of the tumor vessels also profoundly influences the outcome of different immunotherapeutic strategies (10, 11). Moreover, several recent preclinical studies have shown that a combination of immune checkpoint blockade with anti-angiogenic treatment could result in improved outcomes (12, 13). Better understanding of the crosstalk between the angiogenic determinants and immunotherapies may lead to more effective clinical strategies.

In this study, we identified *Myct1* as a direct target of ETS transcription factor ETV2, a critical factor for vascular development, regeneration, and tumor angiogenesis (14–18). We found that although *Myct1* is dispensable for vascular development and homeostasis, it is crucial for tumor progression through the regulation of tumor angiogenesis and tumor immunity. Remarkably, *Myct1* inhibition in combination with anti-PD1 led to dramatic tumor regression. These findings establish a critical role for *Myct1* in modulating the tumor vasculature and remodeling of immune constituents of the tumor microenvironment.

Results

Myct1 is a direct target of ETV2 and is an angiogenic regulator gene.

We first analyzed the expression profiles of more than 8,000 human cancer patients (from thirteen different cancer types) from The Cancer Genome Atlas (TCGA) database. We generated a list of the top 20 potential angiogenesis regulatory genes (Table 1 and table S1), whose expression correlates with “seed genes” that are well characterized in angiogenesis and endothelial cell (EC) biology (See Materials and Methods for details; table S2) (19–21). Comparing this list with the ETS transcription factor ETV2 transcriptional target genes (15), we found *Flt1, Myct1, Ptprb, and S1pr1* as top potential angiogenesis regulatory genes downstream of ETV2. Unlike the other genes, *Myct1* has never been implicated in angiogenesis; hence, we identified *Myct1* as a potential angiogenic gene. Consistent with this idea, we found that *Myct1* expression was mostly restricted to ECs (fig. S1A). Next, we performed a gene set variation analysis with TCGA-derived patient datasets using a signature of genes upregulated during angiogenesis to generate an “Angiogenic score” for every patient (table S3) (22). We found that *MYCT1* expression was significantly ($p<0.05$) correlated with the “Angiogenic score” in all cancers analyzed (Fig. 1A and fig. S2A). Moreover, we found increased *Myct1* expression in the tumor-ECs compared to the non-tumor-ECs in mouse models (Fig. 1B). In line with this, our analysis of a recently published single-cell RNA sequencing dataset (GSE110501) (23) on the heterogeneous mouse tumor stromal population revealed that *Myct1* expression is observed exclusively in the tumor-ECs

(fig. S3A–C). Additionally, in the same dataset, compared to the EC population from a healthy heart, the tumor-EC population had a higher number of cells that expressed *Myct1* (fig. S3D). Together, these observations suggest that *Myct1* plays a role in tumor angiogenesis/vasculature in both human cancers and mouse tumors.

We identified one potential ETV2 binding site in the *Myct1* promoter region by analyzing previously published ETV2 ChIP-Seq data (Fig. 1C) (15). This binding was validated by ChIP-qPCR (Fig. 1D) (14). Only ETV2 and no other ETS transcription factors, such as FLI1 and ERG, activated different luciferase constructs made with varying sizes of the *Myct1* promoter region, all containing the ETS binding motif. Mutations of the ETS binding motifs reduced luciferase activity, implying that these sites were critical for ETV2 binding (Fig. 1E, 1F, and S4A). In vitro overexpression of *Myct1* rescued the tube-like structure formation, sprouting, and migration defects observed in the *Etv2* deficient ECs (fig. S4B–E). Finally, *Myct1* was downregulated in the tumor-ECs of the *Etv2* conditional knockout (KO) mice (Fig. 1G) and intra-tumoral lentiviral *Myct1* expression rescued impaired tumor growth and angiogenesis observed in *Etv2* deficiency (17) (Fig. 1H and 1I). In this experiment, intra-tumoral lentiviral *Myct1* injection resulted in enforced expression of *Myct1* in ECs, as well as in tumor cells and hematopoietic cells (fig. S4F). To assess whether the observed phenotypic rescue is from non-endothelial enforced *Myct1* expression, we generated *Myct1* overexpressing Lewis lung carcinoma (LLC) tumor cells and found that there is no growth advantage for these *Myct1* overexpressing tumor cells in the wild-type (WT) mice (fig. S4G and S4H). Additionally, tumor growth patterns in our bone-marrow chimeric mice suggest that *Myct1* expression in hematopoietic cells does not contribute to tumor growth (as described below; see Fig. 2G–J). Together, these results suggested that *Myct1* was a direct target gene of ETV2 that regulates the angiogenic functionalities of ECs.

Myct1 is dispensable for vascular development and homeostasis in mice and zebrafish.

We generated *Myct1*$^{-/-}$ (*Myct1* KO) mice by utilizing the CRISPR/CAS9 technology. Briefly, we designed gRNA to target the first exon of the *Myct1* gene and injected it together with *Cas9* mRNA into fertilized eggs (Details in the Materials and Method section; fig. S4I–K). By crossing the candidate knockout founder to wild-type mice, we generated heterozygous (*Myct1*$^{+/-}$) offspring and obtained *Myct1* KO mice from brother-sister matings. *Myct1* expression was undetected in the ECs isolated from the lungs of the KO animals (fig. S4L), confirming the efficient deletion of the gene. *Myct1* KO mice appeared normal and exhibited histologically regular vasculature in different organ beds. Vital cardiovascular parameters (Fig. 1J), compliance profiles of the ascending aorta and carotid artery (Fig. 1K), and clinically relevant cardiac functions (Fig. 1L) were similar between the *Myct1* KO and littermate control mice. Similarly, *myct1* zebrafish morphants showed minimal defects in vascular development (fig. S4M). Together, these observations suggested that *Myct1* was dispensable for vascular development, maintenance, and homeostatic functions.

Myct1 is required for efficient tumor growth and tumor vasculature in multiple mouse models.

Since high *Myct1* expression is observed in tumor ECs, we determined whether *Myct1* deficiency has any impact on tumor growth by employing five different (one transgenic, three subcutaneous transplantation, and one orthotopic transplantation) mouse models of cancer. For the transgenic model, we developed MMTV-PyMT; *Myct1*$^{-/-}$ mice as a spontaneous breast cancer model and tracked the development and progression of the tumor in the mammary gland (fig. S5A). For transplantation models, we subcutaneously transplanted Lewis lung carcinoma (LLC-GFP) (17), B16F10 melanoma, and 1956 sarcoma tumor cells (24) and orthotopically transplanted PyMT-BO1 mammary tumor cells (25) to the mammary fat pad as described previously (17, 26). Compared to WT mice, *Myct1* KO mice showed retarded tumor growth in all five of the tumor models; the growth restricted tumors had reduced counts of tumor vessels, which had better pericyte coverages (Fig. 2A–2F and fig. S5B–S5F). Moreover, *Myct1* KO mice exhibited subsided intra-tumoral hypoxia (fig. S6A), improved vascular perfusion (fig. S6B), and reduced vascular leakage (fig. S6C). These data demonstrated that although not essential for vascular development and maintenance, *Myct1* deficiency led to reduced tumor growth and normalization of tumor vessels.

Endothelial *Myct1* is critical for tumor growth in mice.

While *Myct1* expression was mostly restricted to the ECs, *Myct1* was also expressed in hematopoietic stem and progenitor cells (fig. S1A. See also fig. S3A–C) (27–29). To evaluate whether the observed growth restrictive phenotype is dependent on EC-specific *Myct1*, we generated two distinct bone marrow chimeras: ‘WT hematopoietic/*Myct1* KO background’ and ‘*Myct1* KO hematopoietic/WT background’ (fig. S7A) mice. ‘WT hematopoietic/*Myct1* KO background’ chimeric mice exhibited impaired tumor growth and vascular network formation, a phenotype similar to *Myct1* KO mice (Fig. 2G and 2H). However, ‘*Myct1* KO hematopoietic/WT background’ chimeric mice exhibited tumor growth comparable to WT mice (Fig. 2I and 2J). Moreover, endothelial-specific *Myct1* deletion in mice (Cdh5-cre *Myct1*$^{f/f}$) recapitulated the global *Myct1* KO phenotype of retarded tumor growth and reduced angiogenesis, together suggesting that hematopoietic *Myct1* expression was dispensable for tumor progression (fig. S7B–D).

To investigate whether *Myct1* plays any role(s) in tumor cells, we assessed *Myct1* expression in the tumor cell lines utilized earlier in the present study and found that *Myct1* expression was not detectable (fig. S8A). To investigate whether synthetic *Myct1* expression in tumor cells contributes to growth, we genetically modified LLC tumor cells with either *Myct1* shRNA or *Myct1* overexpressing lentivirus and the PyMT-BO1 tumor cells with *Myct1* siRNA. We found that either *Myct1* siRNA or shRNA treatment or enforced expression of *Myct1* in the tumor cells did not play any role in tumor growth kinetics (fig. S8B–E). Additionally, tumor explants from neither the WT nor the *Myct1* KO MMTV-PyMT mice exhibited any growth defects in the WT recipient mice. However, explants from both types of mice showed tumor growth defects in the *Myct1* KO recipient mice (fig. S8F). Together these data suggest that *Myct1* function in the observed phenotype is tumor cell independent. We also modified a human fibroblast cell line (BJ-5ta) that does not express

MYCT1 by treating with *MYCT1* shRNA or enforcing the expression of *MYCT1* with lentivirus. We found that neither of the modifications impacted the growth kinetics and angiogenic sprouting of the fibroblasts (fig. S8G–I). Collectively, these data suggested an endothelial-specific role of *Myct1* in tumor growth and angiogenesis.

Myct1 is also required for vascular regeneration in mice.

To investigate whether *Myct1* is required exclusively for tumor angiogenesis, we utilized a mouse hindlimb ischemia injury model as described previously (18). We found that following the injury, *Myct1* KO mice had a lower blood perfusion recovery and neovascularization of the injured area compared to WT mice (fig. S8J and S8K), suggesting that the *Myct1* requirement is not exclusive to tumor angiogenesis - other forms of neovascularization also require *Myct1*.

MYCT1 interacts with ZO1 and regulates EC motility through actin cytoskeleton in vitro.

Because very little is known about the cellular functions of *Myct1*, we first assessed the subcellular localization of MYCT1 in ECs. To this end, we generated mouse cardiac EC lines (MCEC) expressing either N-terminal HA-tagged or C-terminal FLAG-tagged mouse *Myct1* (Fig. 3A). Flow cytometric analysis revealed that in the intact cells, whereas the anti-HA antibody recognized HA-MYCT1, the anti-FLAG antibody did not recognize MYCT1-FLAG. On the contrary, both the antibodies recognized HA-MYCT1 and MYCT1-FLAG in permeabilized cells (Fig. 3A). Immunofluorescence with anti-HA and anti-FLAG antibodies showed that MYCT1 is indeed present at the plasma membrane, as well as in the cytoplasm, where it was found colocalized mainly with $GM130^+$ and $GIANTIN^+$ Golgi apparatus (fig. S9A–C). Collectively, these results demonstrated that MYCT1 is a membrane-spanning protein with an extracellular N-terminal and an intracellular C-terminal, consistent with a previous structural prediction based on bioinformatic analysis of MYCT1 (30).

We next developed *Myct1* knockdown (KD) MCEC cells (fig. S9D) and assessed EC functionalities. We did not observe any proliferative or maintenance disparity compared to the parental cells, as supported by the similar cell cycle distribution between parental and *Myct1* KD cells (Fig. 3B and fig. S9E). However, *Myct1* KD MCEC cells showed defects in tube-like structure formation in the Matrigel assay (Fig. 3C) and tumor spheroid/EC co-culture assay (Fig. 3D and fig. S9F). *Myct1* KD MCEC cells also displayed defects in sprout formation on the fibrin gel matrix (Fig. 3E and 3F). Additionally, *Myct1* KD MCEC cells lost their migratory characteristics, as shown in the Boyden chamber tumor-chemotaxis assay (Fig. 3G and fig. S9G) and wound-closure assay (Fig. 3H). Importantly, parental cells utilized in these studies did not show any difference compared to the sham shRNA or empty vector control transduced cells (fig. S9H and S9I). Together, these findings suggested that while *Myct1* is not required for the steady-state maintenance of ECs, it is essential for ECs responses in the angiogenic environment.

Different phases of angiogenesis, such as sprouting, migration, and tube-like-structure formation, require EC alignment and directional movement in response to angiogenic cues (31). To understand why *Myct1* KD ECs show defective migratory properties in the angiogenic environment, we assessed the downstream effectors of *Myct1* in regulating EC

motility. Specifically, we extracted RNA from sprouts formed in the fibrin gel matrix (see Fig. 3E) and performed a PCR array for genes that regulate cellular motility (fig. S9J). Genes that regulate actin cytoskeleton dynamics and cell adhesion turnover such as *Capn2, Actin, Actinr2 and 3, Cfl1, Rdx, Myl12a*, and *Wasf1* were downregulated in the *Myct1* KD MCEC sprouts (fig. S9J). *Rhoa* and *Rhoc*, which are required for the formation of actin stress fibers, cell retraction following protrusions, and overall movement (32), were also downregulated (fig. S9J), implying that Rho GTPase signaling is defective in *Myct1* KD cells. Intriguingly, elements of RAC signaling, such as *Rac1, Arhgef7*, and *Stat3*, were upregulated in the *Myct1* KD sprouts, suggesting an unbalanced hyperactivation of RAC signaling, which regulates the formation of leading-edge protrusion during cell movement (32). Consistent with this idea, *Myct1* KD MCEC cells in both 2D culture (Fig. 3I) and scattered 3D tube structures (fig. S9K) formed virtually no stress fibers, which are critical for cellular contractility-relaxation, adhesion, and migration (33). Notably, *Arhgdia*, a Rho GDP dissociation inhibitor that keeps Rho GTPase proteins in their inactive forms (34), was highly upregulated in the *Myct1* KD MCEC sprouts (fig. S9J), again implying a dysregulated Rho GTPase signaling. Congruent with this idea, *Arhgdia* knockdown moderately rescued the *Myct1* KD MCEC phenotype (fig. S9L–N).

Next, we characterized MYCT1 binding partners by taking a target-directed approach. Using proteomics analysis, we identified ZO1 (Zona Occludens 1, also known as tight junction protein 1) and CKAP4 as potential candidates for binding MYCT1 (Supplementary Excel file 1). We confirmed ZO1 and CKAP4 as binding partners of MYCT1 by utilizing co-immunoprecipitation followed by western blot. Intriguingly, we found that, although ZO1 and CKAP4 do not bind directly to each other, MYCT1 binds both of them together in a complex (Fig. 3J and 3K). Immunofluorescence also supported the interaction between MYCT1 and ZO1 by co-localization (Fig. 3L). A similar binding pattern between MYCT1 and CKAP4 in HEK293T cells was also reported in a previous study (35). Since ZO1 plays a critical role in EC functions such as barrier formation, tension, and migration (36) and RHOA regulates endothelial tight junction maintenance and barrier formation in close association with ZO1 (37), we investigated whether there is a functional interplay between MYCT1, ZO1, and RHOA through a series of combined knockdown and overexpression of these genes in MCEC cells. We found that similar to *Myct1* KD, downregulation of either *Zo1* or *Rhoa* led to impaired sprouting and tube formation of ECs in the angiogenic environment. These angiogenic defects of *Myct1* deficient ECs were partially rescued by *Zo1* overexpression; likewise, *Zo1* deficiency phenotypes were partially rescued by *Myct1* overexpression (Fig. 3M and fig. S10A–C). We observed similar, although to a somewhat lesser extent, interplay between *Myct1* and *Rhoa* as well (Fig. 3M and fig. S10A–C), suggesting that MYCT1-ZO1 complex works in close functional association with RHOA to control the actin cytoskeleton. Intriguingly, both the parental and *Myct1* KD cells responded similarly to VEGF in a fibrin gel sprouting assay, suggesting that *Myct1* might regulate ECs angiogenic functionalities independently of VEGF (fig. S10D). Collectively, these data suggested that MYCT1 regulates directional movement of ECs in the angiogenic environment through controlling actin cytoskeleton dynamics.

Endothelial MYCT1 function is evolutionarily conserved between human and mouse

Mouse MYCT1 protein shares an 85% sequence identity with the human MYCT1 protein (30, 35) (fig. S11A). To determine whether MYCT1 function is conserved between human and mouse, we knocked-down human *MYCT1* in HUVEC (HUVEC hMKD) cells (fig. S11B). Similar to the *Myct1* KD MCEC cells, HUVEC hMKD cells displayed severely impaired tube-like-structure generation, sprout formation, and migration capabilities (Fig. 4A–C). Importantly, enforced expression of mouse *Myct1* almost completely rescued the human *MYCT1* KD defects and vice-versa in vitro (Fig. 4A–F and fig. S11B). Moreover, both the mouse and human MYCT1 overexpression rescued the impaired tumor growth and reduced angiogenesis phenotype of the *Myct1* KO mice in a subcutaneous tumor transplantation model (Fig. 4G, 4H, and fig. S11C). Again, although the lentiviral treatment induced *Myct1* over expression in tumor cells and hematopoietic cells along with the ECs, as we described above (see fig. S8A–I), the observed rescue of the tumor phenotype in this experiment is most likely from endothelial *Myct1*. Together, these data suggest that the MYCT1 function in EC is conserved between human and mouse.

Analysis of mouse tumor endothelial transcriptome reveals *Myct1* regulation of angiogenesis and immune responses.

To better understand the tumor endothelial heterogeneity and the potential roles of *Myct1* in tumor-ECs, we performed single-cell RNA-sequencing on sorted tumor-ECs from the PyMT-BO1 orthotopic tumor bearing WT and Cdh5-cre $Myct1^{f/f}$ mice using the 10X-genomics platform. Unsupervised hierarchical and Seurat cell-clustering analysis (38–41) (using a total of 965 ECs) revealed heterogeneity in the tumor endothelium. We identified distinct clusters of angiogenic, tip-like, stalk-like, proliferating, and transitionary ECs (Fig. 5A, 5B, and fig. S12A). Compared to WT tumor-ECs, *Myct1* KO tumor-ECs had a vastly different transcriptional landscape, as evidenced by the reduced angiogenic and tip-like cell populations that are enriched for biological processes related to growth factor activities and invasive vascularization as per Gene Set Enrichment Analysis (Fig. 5C–H) (42). *Myct1* KO tumor-ECs had increased stalk-like and transitionary cell populations that were enriched for biological processes related to leukocyte transendothelial migration, oxidative phosphorylation, and antigen presentation and processing (Fig. 5I–N), collectively reflecting on the *Myct1* requirement for aggressive tumor angiogenesis and tumor immune modulation. We applied SCENIC (Single-cell rEgulatory Network Inference and Clustering) (43), which scans co-expression of transcription factors and putative target genes, and found that WT and *Myct1* KO tumor-ECs were in transcriptionally distinct cellular states (Fig. 5O). While angiogenic transcriptional networks were driving the gene expressions in WT tumor-ECs, transcription factors for immune responses were among the prominent transcriptional drivers for gene expressions in *Myct1* KO tumor-ECs (Fig. 5P).

Additionally, we observed similar patterns of transcriptional activities even in the WT tumor-ECs grouped as $Myct1^{high}$ and $Myct1^{low}$ expressing cells in one other tumor model. Briefly, we performed single-cell RNA-sequencing on sorted tumor-ECs from the LLC subcutaneous transplantation tumor model with only WT mice using the 10X-genomics platform. Unsupervised hierarchical cell-clustering analysis (using a total of 1977 ECs) revealed a similar heterogeneity and *Myct1* expression pattern in the tumor-ECs (fig. S13A–

D). Gene Set Variance Analysis for biological activities on the tumor-ECs based on high and low *Myct1* expression revealed a similar enrichment pattern as the WT vs *Myct1* KO tumor-ECs. As such, *Myct1*^{low} ECs were enriched for biological processes related to leukocyte transendothelial migration, whereas *Myct1*^{high} ECs were enriched for processes related to active vascularization (fig. S13E).

Myct1 deficiency leads to increased formation of high endothelial venules (HEV) in mouse tumors and an overall immunostimulatory tumor microenvironment.

While *Myct1* KO mice exhibited reduced tumor vessel formation, we found that they developed more intra-tumoral high endothelial venules (HEV) compared to the WT mice (Fig. 6A and fig. S14A–C). HEVs are specialized vascular structures that mediate large scale lymphocyte extravasation in lymphoid organs and inflammatory sites. In solid tumors, HEVs preferentially facilitate infiltration of $CD8^+$ cytotoxic T lymphocytes (CTL) into the tumor, and their presence is correlated with reduced tumor growth and favorable prognosis in cancer patients (44). The potential role(s) of *Myct1* in leukocyte adhesion and endothelial transmigration (see Fig. 5I–K and fig. S13E) and HEV formation (Fig. 6A and fig. S14A–C) suggested a possible alteration of tumor immune environment in the *Myct1* KO mice. Indeed, flow cytometric analysis revealed that tumors from *Myct1* KO mice exhibited an increase of CTLs and a decrease of immunosuppressive regulatory T cells (Treg), as evident by the increased 'CD8-to-Treg ratios' in all the tumor models (Fig. 6B, 6C and fig. S14D, S14E). Likewise, tumors from *Myct1* KO mice had an increased M1-macrophage population and a decreased M2-macrophage population; further manifested by the increased 'M1-to-M2 ratios' in all the tumor models (Fig. 6B, 6C). Similar to the *Myct1* KO mice, *Etv2* conditional KO mice exhibited normalization of tumor vasculature and an immunostimulatory tumor microenvironment, as evidenced by the increased 'CD8-to-Treg' and 'M1-to-M2' ratios (fig. S14F; also see Fig. 1H, 1I) (17). Intriguingly, this anti-tumor immune environment was reversed to a pro-tumor environment following enforced *Myct1* expression (fig. S14F). Moreover, analysis of TCGA-derived cancer datasets using an immune-cell-deconvolution algorithm from CIBERSORT (45) revealed similar trends. Tumor samples with low *MYCT1* expression showed decreased *FOXP3* expression, a marker for regulatory T cells, and increased 'M1-to-M2 ratio' compared to the high expression group (Fig. 6D). Additionally, in some cancer types, tumor samples with low *MYCT1* expression also exhibited higher frequencies of activated natural killer (NK) cells and activated dendritic cells (DC) (fig. S14G). Collectively, these observations suggested that *Myct1* deficiency in tumor endothelial cells promotes an anti-tumor immune microenvironment.

Vascular normalization-mediated tumor growth restriction observed in *Myct1* KO mice is dependent on adaptive immunity.

If, indeed, the increased CTLs in *Myct1* KO tumor contributed to the tumor growth restriction, the ablation of CTLs should restore the tumor growth. To this end, we utilized neutralizing antibodies to deplete $CD4^+$ and $CD8^+$ T cell compartments in the tumor-bearing *Myct1* KO mice and found that the tumor growth restriction was completely abrogated (Fig. 6E and fig. S14H), suggesting that the presence of the adaptive immunity was essential for the anti-tumor activity of *Myct1*-mediated tumor vessel normalization. This crosstalk

between tumor vascular control and adaptive immunity was partly IFNγ-mediated. While IFNγ neutralizing antibody abrogated tumor growth restriction phenotype of *Myct1* KO mice, mimicking the $CD4^+$ and $CD8^+$ T cell depletion, recombinant IFNγ treatment partially restored the phenotype in $CD4^+$ and $CD8^+$ T-cell-depleted *Myct1* KO mice (Fig. 6F). Together, our data demonstrate that *Myct1*-mediated tumor vascular control actively shapes the tumor microenvironment through a close engagement with adaptive immunity. Notably, we also observed a small but statistically significant ($p<0.05$) increase in tumor vessels in the $CD4^+$ and $CD8^+$ T cell-depleted *Myct1* KO mice (fig. S14I). This observation was similar in principle to a previous report that depletion of $CD8^+$ T cells was associated with a dramatic increase in tumor microvascular frequency (46). However, the lack of *Myct1* could be the reason why we observed only a modest increase of tumor vasculature even after T cell depletion.

Myct1-deficient ECs promote T cell trafficking and skew macrophage polarization in the angiogenic environment.

Since both the *Myct1* KO and $Myct1^{low}$ tumor-ECs were enriched for leukocyte adhesion and transendothelial migration (Fig. 5I–K and fig. S13E), we evaluated whether *Myct1*-deficient ECs supported more T cell infiltration. By utilizing a modified T cell transendothelial migration assay as described previously (47), we found that $CD8^+$ T cells transmigrated through the *Myct1*-deficient EC barrier more compared to the WT EC barrier (Fig. 6G). However, Treg cells did not display any difference in transmigration between the WT or *Myct1* deficient ECs (fig. S14J). Mechanistically, *Myct1* KO tumor-ECs showed increased expression of endothelial adhesion molecules E-and P-selectin, ICAM-1, and VCAM-1 (Fig. 6H and fig. S14K). Moreover, *Myct1* KO tumor-ECs had increased expression of *Rac1* and associated effector molecules such as *Trio*, *Tiam*, and *Rhog* (Fig. 6H and fig. S14K). This upregulation of the *Rac1*-mediated pathway is crucial as RAC1 inhibition by NSC23766 abrogated the increased T cell migration phenotype (Fig. 6G and fig. S14J). Additionally, tumor endothelium is known to express immune-suppressor molecules, such as PDL1, PDL2, Fas ligand, and TRAIL (48–51). We found that the expression of Fas ligand (*Faslg*), which can induce apoptosis of infiltrating $CD8^+$ T cells by binding to the cognate FAS receptor (51), was downregulated in *Myct1* KO tumor-ECs (Fig. 6I). We observed a similar trend in the tumor samples with low *MYCT1* expression compared to the samples with high *MYCT1* expression in some human cancer types (Fig. 6J). Finally, we investigated whether *Myct1* expression in tumor endothelium had any direct impact on macrophage polarization. In the presence of respective M1 or M2 polarizing cytokines, *Myct1*-deficient ECs promoted more M1-like and less M2-like macrophage polarization from monocytes (Fig. 6K). Intriguingly, tumor-ECs in *Myct1* KO mice exhibited reduced expression of *Nos2* and *Nos3* (Fig. 6L and fig. S14L), which have been shown to affect M1- and M2-macrophage polarization (52–54), suggesting a potential role for nitric oxide synthase (NOS) in the observed anti-tumor macrophage skewing. Together, this series of investigations provided a mechanistic explanation for the observed anti-tumor T-cell and macrophage remodeling phenotype in the *Myct1* KO mice.

Targeting of *Myct1* improves anti-PD1 immunotherapy outcomes in mice.

The success of the immune checkpoint blockade-mediated immunotherapeutic approach partially relies on the presence of CTLs in the tumor microenvironment. Since our data show that *Myct1*-deficient tumor endothelium promotes CTL infiltration, addition of anti-PD1 to prevent CTL exhaustion might provide a synergistic and superior treatment outcome. As such, we assessed the efficacy and usefulness of the combined anti-*Myct1* and anti-PD1 treatment approaches in both anti-PD1-responsive and anti-PD1-refractory tumor models. First, we utilized an anti-PD1-responsive 1956 sarcoma subcutaneous transplantation tumor model that responds completely to an early-onset scheme of anti-PD1 treatment, but not to late-onset schemes (24). To this end, we validated different modalities of anti-PD1 therapy in this tumor model and found that a late-onset treatment starting from 9-days post-tumor transplantation did not result in total regression, but somewhat slowed tumor progression with eventual complete relapse of the tumor in WT mice (Fig. 7A). We treated the tumor-bearing *Myct1* KO mice with this late-onset anti-PD1 scheme and observed dramatic tumor regression within 12 days of treatment initiation (Fig. 7B). This short-term regression led to complete tumor regression in all but one treated mouse (7 out of 8) (Fig. 7C). Supporting our observation that endothelial-specific *Myct1* regulates the tumor growth and angiogenesis, Cdh5-cre $Myct1^{f/f}$ mice demonstrated a similar tumor regression with this late-onset anti-PD1 treatment scheme (fig. S15A). To determine whether a systemic anti-*Myct1* approach confers similar anti-tumor activity, we utilized a *Myct1* directed siRNA-peptide nanoparticle treatment approach in WT mice (17, 55) either alone or in combination with DC101 (a VEGF receptor 2 (VEGFR2) blocking antibody) and/or anti-PD1, following a similar late-onset treatment scheme (Fig. 7D). We found that combined anti-PD1 and anti-*Myct1* treatment restricted tumor progression in all the treated mice (Fig. 7D), with a complete regression in 25% of the mice (2 out of 8) (Fig. 7E). In comparison, combined anti-PD1 and DC101 treatment also produced significant ($p<0.05$) short-term tumor growth restriction, though to a somewhat lesser extent (Fig. 7D), with an eventual relapse of tumor growth in all mice (Fig. 7E). Remarkably, anti-PD1 treatment with the dual blockade of *Myct1* and VEGFR2 resulted in complete tumor regression in all of the treated mice (fig. 7E). Since combined *Myct1* siRNA and anti-PD1 treatment resulted a complete tumor regression in 2 out of 8 mice (Fig. 7E), while anti-PD1 treatment in *Myct1* KO mice led to complete tumor regression in 7 out of 8 mice (Fig. 7C), we assessed whether this was due to a sub-optimal *Myct1* siRNA treatment. We utilized an extended anti-*Myct1* treatment approach that started before the onset and continued after the termination of the anti-PD1 treatment. We found that this prolonged anti-*Myct1* treatment resulted in the restriction of tumor progression for a longer period, with about 60% mice showing complete tumor regression (14 out of 24 mice) (Fig. 7F).

Next, we assessed whether *Myct1* targeting could sensitize anti-PD1-refractory tumors. Here, we utilized an orthotopic breast tumor model with PyMT-BO1 tumors that do not respond to anti-PD1 treatment (Fig. 7G). We treated tumor-bearing WT mice with *Myct1*-directed siRNA-peptide nanoparticles either alone or in combination with DC101 and/or anti-PD1. Although DC101 failed to induce any sensitivity to anti-PD1 treatment, combined anti-*Myct1* and anti-PD1 treatment resulted in a substantial short-term tumor regression (Fig. 7H), with complete tumor regression in 43% of the treated mice (3 out of 7) (Fig. 7I).

Intriguingly, similar to the 1956 sarcoma model, dual blockade of *Myct1* and VEGFR2 with anti-PD1 treatment generated both the maximal short-term tumor restriction and long-term complete tumor regression (7 out of 8 mice) (Fig. 7H and 7I), suggesting that the collective blockade of both the VEGF and MYCT1 pathways might provide better and longer-lasting vascular control, resulting in improved outcomes with anti-PD1 immunotherapy in both sensitive and refractory tumor models.

Dormant tumor cells can reinitiate tumor growth after treatment (56–58). To address if dormant tumor cells still existed in these transplant tumor models after anti-*Myct1* and anti-PD1 treatment, we treated the tumor-regressed mice (pooled from the experiments with 1956 sarcoma tumor model described in Fig. 7E and 7F) with monoclonal neutralizing antibodies against CD4, CD8, and IFNγ, three major components of adaptive immunity. None of the tumor-regressed mice developed any tumor mass after the alleviation of the immune surveillance for a period of over 90 days (fig. S15B), suggesting that anti-PD1 treatment combined with anti-*Myct1* targeting, with or without other anti-angiogenics, not only brought complete tumor regression but also destroyed any potential dormant tumor cells residing in the equilibrium phase. Intriguingly, re-challenging both the tumor-regressed mice (pooled from the experiment with PyMT-BO1 tumor model described in Fig. 7H) and naïve control mice with the PyMT-BO1 tumor cells resulted in unrestrained tumor growth without any statistical difference (fig. S15C), suggesting that anti-*Myct1* and anti-PD1 combination treatment did not induce long-lived immunological memory.

To further understand how *Myct1*-directed siRNA-peptide nanoparticle treatment improves the outcome of the anti-PD1 immunotherapy, we harvested and analyzed tumors seven days after treatment initiation in the anti-PD1 refractory PyMT-BO1 tumor model, at a time when the tumors just started to respond to combination treatment (fig. S16A). Flow cytometric analysis revealed that anti-*Myct1* treatment increased CTLs and M1 macrophages, while reducing the number of Treg cells and M2 macrophages. Conversely, anti-PD1 treatment increased the percentage of Granzyme B+ CTLs, but did not alter the immune microenvironment. Notably, anti-*Myct1* and anti-PD1 combined treatment increased both the influx of CTLs and the percentage of Granzyme B+ CTLs, suggesting that the combination treatment produces considerably superior tumor control due to the additive nature of the individual treatments on CTLs (Fig. 8A). Immunofluorescence observations supported the conclusion that anti-*Myct1* treatment reduced angiogenesis, improved vascular normalization, and increased the infiltration of CD8+ T cells (Fig. 8B–E). Intriguingly, although the siRNA-peptide nanoparticle treatment downregulated *Myct1* expression in both the tumor and non-tumor endothelium (fig. S16B), unlike in the tumor masses, there were no alterations in the immune constituents of the non-tumor tissues (fig. S16C). We observed a similar modification of immune constituents of the tumor masses in the *Myct1* KO mice with the anti-PD1 treatment, supporting the notion of the additive nature of the treatments (fig. S16D and S16E). Downregulation of *Myct1* by the nanoparticles led to the upregulation of several adhesion molecules, among which *Selp* and *Icam1* reached statistical significance ($p<0.05$), only in the tumor endothelium but not in the non-tumor tissues (Fig. 8F and fig. S17A), corroborating the observations in the *Myct1* KO mice (see Fig. 6H). Importantly, *Myct1*-directed siRNA-peptide nanoparticle treatment largely did not induce any non-specific immune responses in either the tumor-infiltrating hematopoietic cells or tumor cells

(Fig. 8F, fig. S17B, and S17C). Collectively, these observations suggest that *Myct1* targeting generates tumor-EC-focused changes that allows anti-PD1 treatment to mount more effective anti-tumor responses.

Discussion

Myct1 was first identified as a direct target gene of c-MYC in myeloid cells, as well as in laryngeal squamous cell carcinoma cells, in the context of c-MYC overexpression (59, 60). However, analysis of published scRNA sequencing datasets from different mouse organs revealed that *Myct1* expression is mostly restricted to ECs and hematopoietic stem and progenitor cells. We have demonstrated that *Myct1* is highly expressed in tumor ECs and is a regulator of angiogenesis. We found that *Myct1* is not required for blood and vascular development. Instead, *Myct1* seems to regulate acute angiogenic demand in pathological conditions such as cancer. Notably, data from human patients with varying *MYCT1* expression across multiple different cancer types also suggest that *MYCT1* is positively correlated with the angiogenic status of the cancers. Particularly, we show that MYCT1 regulates EC motility by interacting with ZO1 and CKAP4 and modulating Rho GTPases and actin cytoskeleton. It will be necessary to further delineate the crosstalk among MYCT1, ZO1, Rho GTPases, and CKAP4 in regulating the actin cytoskeleton and EC motility.

Myct1 deficient tumor vasculature is characterized by having more HEVs, facilitating CTLs infiltration, and promoting anti-tumor macrophage polarization. Tumor vessels inhibit CTLs activation and promote apoptosis of the infiltrating immune cells in part by upregulating immunosuppressive molecules, PDL1, PDL2, Fas ligand, and TRAIL (48–51). We found that *Myct1* deficient ECs downregulate the expression of Fas ligand. We also found a similar trend with human cancers with reduced *MYCT1* expression. Our data suggest that *Myct1* deficient endothelium promotes an immunostimulatory microenvironment by enhancing CTLs infiltration and presumably by preventing CTLs apoptosis. Moreover, it has been reported that inducible-NOS (NOS2) inhibits the M1-macrophage population, whereas endothelial-NOS (NOS3) promotes the M2-macrophage polarization (52–54). Notably, the expressions of *Nos2* and *Nos3* were decreased in *Myct1* deficient ECs, suggesting that enhanced anti-tumor macrophage polarization in *Myct1* deficient tumor microenvironments may, in part, through the regulation of NO production of ECs. These findings collectively provide mechanistic insights into *Myct1* deficient tumor vessels contributing to an immunostimulatory microenvironment.

Vascular normalization has been implicated to influence local tumor immune environment (61, 62). However, the molecular targets like VEGF and associated pathways also impact the immune cells in an endothelial cell-independent manner (63–66), raising a possibility of synergistic and/or independent effect rather than a sole consequence of vascular normalization on the tumor immune components. *Myct1* targeting in endothelial cells leading to an anti-tumor microenvironment provides more definitive evidence for endothelial regulation of tumor immunity in mice. This data is consistent with the human cancer datasets that show the increased presence of immunostimulatory components in tumors with lower *MYCT1* expression. Our finding supports the emerging notion that combined vascular and immune control would provide a synergistic anti-tumor activity (3, 48, 67–69). Indeed,

our data demonstrate that targeting *Myct1* improves the response to anti-PD1 therapy in treatment-responsive and -refractory tumors. Importantly, we observed that combined *Myct1* and VEGF targeting with anti-PD1 treatment produced a superior tumor control, suggesting a potential synergy between *Myct1* and VEGF pathways.

Our study's limitations include that our data on *Myct1* expression in tumor endothelium is confined to RNA, not protein. Additionally, our data on immune modulation are limited to CTL infiltration and M1 polarization. Global changes in tumor immunity by endothelial-specific *Myct1* deficiency need to be further elucidated to better understand the crosstalk between angiogenesis and tumor immunity. Lastly, while siRNA-nanoparticle-mediated *Myct1* targeting has provided proof of concept, it would be valuable to develop and validate an antibody-mediated MYCT1 blocking approach to realize the therapeutic potential of MYCT1 inhibition.

In summary, we have identified *Myct1* as a regulator of tumor angiogenesis. *Myct1*-deficient ECs display suboptimal angiogenesis, facilitate HEV formation, enhance robust CTL infiltration, and promote inflammatory M1 macrophage polarization. Anti-PD1 antibody treatment in the context of *Myct1* inhibition augments complete tumor elimination in mouse models. We propose that combined *Myct1*-inhibition and immunotherapy might become a treatment regimen for cancer patients.

Materials and Methods

Study design

The goal of the study was to investigate the role of *Myct1* as a regulator of tumor angiogenesis and anti-tumor immunity and to characterize the mechanism of this regulation. The Cancer Genome Atlas (TCGA) datasets for thirteen different cancer types were analyzed to identify *Myct1* as an angiogenic gene downstream of *Etv2* (14, 19, 20, 22, 70). *Myct1* requirement for tumor growth, angiogenesis, and antitumor immunity was assessed by using different preclinical mouse models of cancer (18, 26, 57, 71–76). Potential correlation between endothelial *Myct1* expression and the immune output in the human tumor microenvironment was evaluated by analyzing cancer datasets using the CIBERSORT deconvolution algorithm (45). Using various in vitro assays, the role(s) of *Myct1* in endothelial cells and the underlying mechanisms for regulating anti-tumor immunity were rigorously investigated (17, 77–79). Lastly, using both the knockout mice and siRNA-peptide nanoparticle mediated approach (17), the efficacy of *Myct1* inhibition for treating tumors in combination with anti-PD1 immunotherapy was evaluated. For animal studies, the minimum number of subjects used in any experiments was 5/group to attain a statistical significance of $p<0.05$ with a power of at least 80%, considering the mean differences between experimental groups would be >20% and the pooled standard deviation would be ~20%. For in-vitro experiments, the anticipated mean difference was even more, and hence the sample size was kept at 3 or more/group. Age- and sex-matched mice were randomly assigned into groups in all experiments except experiments utilizing both the genetic and orthotopic breast tumor models, where only female mice were used. The investigators were not aware of the group allocation until the treatment, data collection, and data analysis were done. All experimental data were reliably reproduced in two or more individual biological

replicates unless indicated otherwise. No data were excluded from analysis. Sample sizes, biological replicates, and statistical methods are provided in the corresponding figure legends. Primary data are reported in supplementary data files S1 and S2.

Mice

Myct1$^{-/-}$ (*Myct1* KO) and Cdh5-Cre;*Myct1*$^{f/f}$ mice were generated at Washington University in St. Louis and Emory University, respectively. MMTV-PyMT mice were a gift from Mikala Egeblad, Cold Spring Harbor Laboratory, and crossed with *Myct1* KO mice to generate *Myct1* KO in the presence of MMTV-PyMT transgene (MMTV-PyMT *Myct1*$^{-/-}$) at Washington University in St. Louis. The details of the mice generation can be found in the Supplementary Materials and Methods section. Animal husbandry, generation, handling, and experimentation were done in accordance with protocols approved by the Institutional Animal Care and Use Committee of Washington University School of Medicine in St. Louis.

Mouse tumor models

MMTV-PyMT transgenic mice were utilized to generate a spontaneous model of breast cancer, where MMTV-LTR drives the expression of mouse mammary gland-specific polyomavirus middle T-antigen. For tumor transplantation studies, LLC-GFP, B16F10 melanoma, and 1956 sarcoma tumor cells were injected subcutaneously to the back of the mice. PyMT-BO1 tumor cells were injected orthotopically to the mammary fat pad of the female mice. The details regarding the transplantation procedures, tumor growth monitoring, different treatment schemes, and downstream flow cytometry, immunofluorescence, and RNA expression analysis of the tumor masses can be found in the Supplementary Materials and Methods section.

Cell lines

Mouse cardiac endothelial cells (MCEC) and human umbilical vein endothelial cells (HUVEC) were purchased from CELLutions Biosystems Inc. (Cat: CLU510) and ATCC (Cat: ATCC CRL-1730), respectively. Overexpressing and shRNA lentiviral particles were utilized to generate different genetically modified overexpressing and knockdown stable cell lines. Further details about the cell culture conditions, lentiviral clones, production of lentiviral particles, antibiotic selection, and different treatment schemes for in vitro experiments are provided in the Supplementary Materials and Methods section.

Single-cell RNA sequencing

Endothelial cells sorted by flow cytometry from the tumor masses were loaded on a Chromium Single Cell Instrument (10X Genomics) to generate single-cell GEMs. Single-cell RNA-seq libraries were prepared using version 2 Chromium Single-cell 3′ Library, Gel Bead & Mutiplex Kit (10X Genomics). Sequencing was performed on Illumina NextSeq2500 and mapped to the mouse genome (build mm10) using CellRanger software (10x Genomics, version 2.1.1). Sequencing data is available as GSE157879 and GSE146819. Further details about the sequencing data quality control, normalization, integration, and downstream analysis can be found in the Supplementary Materials and Methods section.

Statistical Analysis

GraphPad Prism 8 software was used for performing statistical analysis and generating graphs/plots. Data are presented as mean with standard deviation for all the measurements. Statistical significance was determined by two-tailed unpaired Student's *t*-test (for two groups) and One-way ANOVA with Tukey's multiple comparison test (for more than two groups). Non-parametric tests were used for non-log transformed gene expression data from the TCGA database. $p<0.05$ was considered statistically significant.

Supplementary Material

Refer to Web version on PubMed Central for supplementary material.

Acknowledgements

We thank Mikala Egeblad at Cold Spring Harbor Laboratory for the generous gift of the MMTV-PyMT mice. We want to thank our colleagues at Washington University, Kory Lavine for MCEC cells, Andrew Yoo for BJ-5ta cells, Katherine Weilbaecher for PyMT-BO1-GFP-Luc cells, Luis Batista for pCDH-(LB12-FLAG-TERT)-EF1-NEO plasmid. We thank Robert D. Schreiber at Washington University for 1956 sarcoma cells and helpful suggestions with experimental design and data interpretation. We also want to thank Alexander S Krupnick at the University of Virginia for providing LLC-GFP cells. We thank Mike White and the Genome Engineering and iPSC Center (GEIC) at Washington University in St. Louis for the generation of *Myct1* KO mice using CRISPR/CAS9 technology. We also thank Washington University Center for Cellular Imaging (WUCCI) and Pathology FACS core for providing access to the light microscopes and FACS facility, respectively. We thank Attila Kovacs and Carla J. Weinheimer of the Mouse Cardiovascular Phenotyping Core at Washington University School of Medicine for the echocardiogram analysis.

Funding:

This work was supported by the NIH grants R01HL149954 (to K.C.), R01HL55337 (to K.C), R01HL119291 (to C.P), and K08HL135400 (to C.M.H), Children's Heart Research and Outcomes Center and Children's Healthcare of Atlanta 00060337 (to C.P.) and Mallinckrodt Challenge Grant (to K.C. and D.H.F.).

References

1. Folkman J, Tumor angiogenesis: therapeutic implications. N. Engl. J. Med 285, 1182–1186 (1971). [PubMed: 4938153]
2. Chung AS, Ferrara N, Developmental and Pathological Angiogenesis. Annual Review of Cell and Developmental Biology 27, 563–584 (2011).
3. Hanahan D, Weinberg RA, Hallmarks of Cancer: The Next Generation. Cell 144, 646–674 (2011). [PubMed: 21376230]
4. Ye W, The Complexity of Translating Anti-angiogenesis Therapy from Basic Science to the Clinic. Developmental Cell 37, 114–125 (2016). [PubMed: 27093081]
5. Bergers G, Hanahan D, Modes of resistance to anti-angiogenic therapy. Nat. Rev. Cancer 8, 592–603 (2008). [PubMed: 18650835]
6. Ferrara N, Adamis AP, Ten years of anti-vascular endothelial growth factor therapy. Nat Rev Drug Discov 15, 385–403 (2016). [PubMed: 26775688]
7. Lee S, Chen TT, Barber CL, Jordan MC, Murdock J, Desai S, Ferrara N, Nagy A, Roos KP, Iruela-Arispe ML, Autocrine VEGF Signaling Is Required for Vascular Homeostasis. Cell 130, 691–703 (2007). [PubMed: 17719546]
8. Yang Y, Zhang Y, Cao Z, Ji H, Yang X, Iwamoto H, Wahlberg E, Lanne T, Sun B, Cao Y, Anti-VEGF- and anti-VEGF receptor-induced vascular alteration in mouse healthy tissues. Proc Natl Acad Sci U S A 110, 12018–12023 (2013). [PubMed: 23818623]

9. Dammeijer F, Lau SP, van Eijck CHJ, van der Burg SH, Aerts J, Rationally combining immunotherapies to improve efficacy of immune checkpoint blockade in solid tumors. Cytokine Growth Factor Rev 36, 5–15 (2017). [PubMed: 28693973]
10. Chauhan VP, Chen IX, Tong R, Ng MR, Martin JD, Naxerova K, Wu MW, Huang P, Boucher Y, Kohane DS, Langer R, Jain RK, Reprogramming the microenvironment with tumor-selective angiotensin blockers enhances cancer immunotherapy. Proc Natl Acad Sci U S A 116, 10674–10680 (2019). [PubMed: 31040208]
11. Chen IX, Chauhan VP, Posada J, Ng MR, Wu MW, Adstamongkonkul P, Huang P, Lindeman N, Langer R, Jain RK, Blocking CXCR4 alleviates desmoplasia, increases T-lymphocyte infiltration, and improves immunotherapy in metastatic breast cancer. Proc Natl Acad Sci U S A 116, 4558–4566 (2019). [PubMed: 30700545]
12. Schmittnaegel M, Rigamonti N, Kadioglu E, Cassara A, Wyser Rmili C, Kiialainen A, Kienast Y, Mueller HJ, Ooi CH, Laoui D, De Palma M, Dual angiopoietin-2 and VEGFA inhibition elicits antitumor immunity that is enhanced by PD-1 checkpoint blockade. Sci Transl Med 9, (2017).
13. Allen E, Jabouille A, Rivera LB, Lodewijckx I, Missiaen R, Steri V, Feyen K, Tawney J, Hanahan D, Michael IP, Bergers G, Combined antiangiogenic and anti-PD-L1 therapy stimulates tumor immunity through HEV formation. Sci Transl Med 9, (2017).
14. Lee D, Park C, Lee H, Lugus JJ, Kim SH, Arentson E, Chung YS, Gomez G, Kyba M, Lin S, Janknecht R, Lim D-S, Choi K, ER71 Acts Downstream of BMP, Notch, and Wnt Signaling in Blood and Vessel Progenitor Specification. Cell Stem Cell 2, 497–507 (2008). [PubMed: 18462699]
15. Liu F, Li D, Yu YYL, Kang I, Cha M-J, Kim JY, Park C, Watson DK, Wang T, Choi K, Induction of hematopoietic and endothelial cell program orchestrated by ETS transcription factor ER71/ETV2. EMBO reports 16, 654–669 (2015). [PubMed: 25802403]
16. Xu CX, Lee TJ, Sakurai N, Krchma K, Liu F, Li D, Wang T, Choi K, ETV2/ER71 regulates hematopoietic regeneration by promoting hematopoietic stem cell proliferation. J Exp Med 214, 1643–1653 (2017). [PubMed: 28461595]
17. Kabir AU, Lee TJ, Pan H, Berry JC, Krchma K, Wu J, Liu F, Kang HK, Hinman K, Yang L, Hamilton S, Zhou Q, Veis DJ, Mecham RP, Wickline SA, Miller MJ, Choi K, Requisite endothelial reactivation and effective siRNA nanoparticle targeting of Etv2/Er71 in tumor angiogenesis. JCI Insight 3, (2018).
18. Park C, Lee T-J, Bhang SH, Liu F, Nakamura R, Oladipupo SS, Pitha-Rowe I, Capoccia B, Choi HS, Kim TM, Urao N, Ushio-Fukai M, Lee D, Miyoshi H, Kim B-S, Lim D-S, Apte RS, Ornitz DM, Choi K, Injury-Mediated Vascular Regeneration Requires Endothelial ER71/ETV2. Arteriosclerosis, Thrombosis, and Vascular Biology 36, 86–96 (2016).
19. Masiero M, Simoes FC, Han HD, Snell C, Peterkin T, Bridges E, Mangala LS, Wu SY, Pradeep S, Li D, Han C, Dalton H, Lopez-Berestein G, Tuynman JB, Mortensen N, Li JL, Patient R, Sood AK, Banham AH, Harris AL, Buffa FM, A core human primary tumor angiogenesis signature identifies the endothelial orphan receptor ELTD1 as a key regulator of angiogenesis. Cancer Cell 24, 229–241 (2013). [PubMed: 23871637]
20. Liberzon A, Birger C, Thorvaldsdóttir H, Ghandi M, Mesirov JP, Tamayo P, The Molecular Signatures Database (MSigDB) hallmark gene set collection. Cell Syst 1, 417–425 (2015). [PubMed: 26771021]
21. D'Costa NM, Cina D, Shrestha R, Bell RH, Lin YY, Asghari H, Monjaras-Avila CU, Kollmannsberger C, Hach F, Chavez-Munoz CI, So AI, Identification of gene signature for treatment response to guide precision oncology in clear-cell renal cell carcinoma. Sci Rep 10, 2026 (2020). [PubMed: 32029828]
22. Hänzelmann S, Castelo R, Guinney J, GSVA: gene set variation analysis for microarray and RNA-Seq data. BMC Bioinformatics 14, 1–15 (2013). [PubMed: 23323762]
23. Zhao Q, Eichten A, Parveen A, Adler C, Huang Y, Wang W, Ding Y, Adler A, Nevins T, Ni M, Wei Y, Thurston G, Single-Cell Transcriptome Analyses Reveal Endothelial Cell Heterogeneity in Tumors and Changes following Antiangiogenic Treatment. Cancer Res 78, 2370–2382 (2018). [PubMed: 29449267]
24. Vesely M, Tumor Antigens Revealed by Exome Seqeuncing Drive Editing of Tumor Immunogenicity. All Theses and Dissertations (ETDs), (2013).

25. Su X, Esser AK, Amend SR, Xiang J, Xu Y, Ross MH, Fox GC, Kobayashi T, Steri V, Roomp K, Fontana F, Hurchla MA, Knolhoff BL, Meyer MA, Morgan EA, Tomasson JC, Novack JS, Zou W, Faccio R, Novack DV, Robinson SD, Teitelbaum SL, DeNardo DG, Schneider JG, Weilbaecher KN, Antagonizing integrin beta3 increases immune suppression in cancer. Cancer Res 76, 3484–3495 (2016). [PubMed: 27216180]
26. Zhang GL, Zhang Y, Cao KX, Wang XM, Orthotopic Injection of Breast Cancer Cells into the Mice Mammary Fat Pad. J Vis Exp, (2019).
27. Uhlen M, Fagerberg L, Hallstrom BM, Lindskog C, Oksvold P, Mardinoglu A, Sivertsson A, Kampf C, Sjostedt E, Asplund A, Olsson I, Edlund K, Lundberg E, Navani S, Szigyarto CA, Odeberg J, Djureinovic D, Takanen JO, Hober S, Alm T, Edqvist PH, Berling H, Tegel H, Mulder J, Rockberg J, Nilsson P, Schwenk JM, Hamsten M, von Feilitzen K, Forsberg M, Persson L, Johansson F, Zwahlen M, von Heijne G, Nielsen J, Ponten F, Proteomics. Tissue-based map of the human proteome. Science 347, 1260419 (2015). [PubMed: 25613900]
28. Heng TS, Painter MW, The Immunological Genome Project: networks of gene expression in immune cells. Nat Immunol 9, 1091–1094 (2008). [PubMed: 18800157]
29. Schaum N, Karkanias J, Neff NF, May AP, Quake SR, Wyss-Coray T, Darmanis S, Batson J, Botvinnik O, Chen MB, Chen S, Green F, Jones R, Maynard A, Penland L, Pisco AO, Sit RV, Stanley GM, Webber JT, Zanini F, Baghel AS, Bakerman I, Bansal I, Berdnik D, Bilen B, Brownfield D, Cain C, Cho M, Cirolia G, Conley SD, Demers A, Demir K, de Morree A, Divita T, du Bois H, Dulgeroff LBT, Ebadi H, Espinoza FH, Fish M, Gan Q, George BM, Gillich A, Genetiano G, Gu X, Gulati GS, Hang Y, Hosseinzadeh S, Huang A, Iram T, Isobe T, Ives F, Kao KS, Karnam G, Kershner AM, Kiss BM, Kong W, Kumar ME, Lam J, Lee DP, Lee SE, Li G, Li Q, Liu L, Lo A, Lu WJ, Manjunath A, May KL, May OL, McKay M, Metzger RJ, Mignardi M, Min D, Nabhan AN, Ng KM, Noh J, Patkar R, Peng WC, Puccinelli R, Rulifson EJ, Sikandar SS, Sinha R, Szade K, Tan W, Tato C, Tellez K, Travaglini KJ, Tropini C, Waldburger L, van Weele LJ, Wosczyna MN, Xiang J, Xue S, Youngyunpipatkul J, Zardeneta ME, Zhang F, Zhou L, oungyunpipatkul JY, Castro P, Croote D, DeRisi JL, Kuo CS, Lehallier B, Nguyen PK, Tan SY, Wang BM, Yousef H, Beachy PA, Chan CKF, Huang KC, Weinberg K, Wu SM, Barres BA, Clarke MF, Kim SK, Krasnow MA, Nusse R, Rando TA, Sonnenburg J, Weissman IL, Single-cell transcriptomics of 20 mouse organs creates a Tabula Muris: The Tabula Muris Consortium. Nature 562, 367–372 (2018). [PubMed: 30283141]
30. Zhang WD, Chen HX, Wang YX, Chen ZP, Shan ZJ, Xu G, Bioinformatic analysis of c-Myc target from laryngeal cancer cell gene of laryngeal cancer. Journal of cancer research and therapeutics 12, 58–61 (2016). [PubMed: 27072211]
31. Eilken HM, Adams RH, Dynamics of endothelial cell behavior in sprouting angiogenesis. Curr Opin Cell Biol 22, 617–625 (2010). [PubMed: 20817428]
32. Ridley AJ, Schwartz MA, Burridge K, Firtel RA, Ginsberg MH, Borisy G, Parsons JT, Horwitz AR, Cell migration: integrating signals from front to back. Science 302, 1704–1709 (2003). [PubMed: 14657486]
33. Hall A, Rho GTPases and the actin cytoskeleton. Science 279, 509–514 (1998). [PubMed: 9438836]
34. Garcia-Mata R, Boulter E, Burridge K, The ‘invisible hand’: regulation of RHO GTPases by RHOGDIs. Nat Rev Mol Cell Biol 12, 493–504 (2011). [PubMed: 21779026]
35. Wu S, Gui J, Yin X, Pan Q, Liu X, Chu L, Transmembrane domain is crucial to the subcellular localization and function of Myc target 1. Journal of cellular and molecular medicine 20, 471–481 (2016). [PubMed: 26710964]
36. Tornavaca O, Chia M, Dufton N, Almagro LO, Conway DE, Randi AM, Schwartz MA, Matter K, Balda MS, ZO-1 controls endothelial adherens junctions, cell-cell tension, angiogenesis, and barrier formation. J Cell Biol 208, 821–838 (2015). [PubMed: 25753039]
37. Citi S, Guerrera D, Spadaro D, Shah J, Epithelial junctions and Rho family GTPases: the zonular signalosome. Small GTPases 5, 1–15 (2014).
38. Stuart T, Butler A, Hoffman P, Hafemeister C, Papalexi E, Mauck WM, Hao Y, Stoeckius M, Smibert P, Satija R, Comprehensive Integration of Single-Cell Data. Cell 177, 1888–1902.e1821 (2019). [PubMed: 31178118]

39. Butler A, Hoffman P, Smibert P, Papalexi E, Satija R, Integrating single-cell transcriptomic data across different conditions, technologies, and species. Nat Biotech 36, 411–420 (2018).
40. Gribov A, Sill M, Luck S, Rucker F, Dohner K, Bullinger L, Benner A, Unwin A, SEURAT: visual analytics for the integrated analysis of microarray data. BMC Med Genomics 3, 21 (2010). [PubMed: 20525257]
41. Hafemeister C, Satija R, Normalization and variance stabilization of single-cell RNA-seq data using regularized negative binomial regression. Genome Biol 20, 296 (2019). [PubMed: 31870423]
42. Subramanian A, Tamayo P, Mootha VK, Mukherjee S, Ebert BL, Gillette MA, Paulovich A, Pomeroy SL, Golub TR, Lander ES, Mesirov JP, Gene set enrichment analysis: a knowledge-based approach for interpreting genome-wide expression profiles. Proc Natl Acad Sci U S A 102, 15545–15550 (2005). [PubMed: 16199517]
43. Aibar S, González-Blas CB, Moerman T, Huynh-Thu VA, Imrichova H, Hulselmans G, Rambow F, Marine JC, Geurts P, Aerts J, van den Oord J, Atak ZK, Wouters J, Aerts S, SCENIC: single-cell regulatory network inference and clustering. Nat Methods 14, 1083–1086 (2017). [PubMed: 28991892]
44. Martinet L, Garrido I, Filleron T, Le Guellec S, Bellard E, Fournie JJ, Rochaix P, Girard JP, Human solid tumors contain high endothelial venules: association with T- and B-lymphocyte infiltration and favorable prognosis in breast cancer. Cancer Res 71, 5678–5687 (2011). [PubMed: 21846823]
45. Newman AM, Liu CL, Green MR, Gentles AJ, Feng W, Xu Y, Hoang CD, Diehn M, Alizadeh AA, Robust enumeration of cell subsets from tissue expression profiles. Nature Methods 12, 453–457 (2015). [PubMed: 25822800]
46. Tian L, Goldstein A, Wang H, Lo HC, Kim IS, Welte T, Sheng K, Dobrolecki LE, Zhang X, Putluri N, Phung TL, Mani SA, Stossi F, Sreekumar A, Mancini MA, Decker WK, Zong C, Lewis MT, Zhang XH-F, Mutual regulation of tumour vessel normalization and immunostimulatory reprogramming. Nature 544, 250–254 (2017). [PubMed: 28371798]
47. Ding Z, Xiong K, Issekutz TB, Regulation of chemokine-induced transendothelial migration of T lymphocytes by endothelial activation: differential effects on naive and memory T cells. Journal of Leukocyte Biology 67, 825–833 (2000). [PubMed: 10857855]
48. Motz GT, Coukos G, The parallel lives of angiogenesis and immunosuppression: cancer and other tales. Nature Reviews Immunology 11, 702–711 (2011).
49. Rodig N, Ryan T, Allen JA, Pang H, Grabie N, Chernova T, Greenfield EA, Liang SC, Sharpe AH, Lichtman AH, Freeman GJ, Endothelial expression of PD-L1 and PD-L2 down-regulates CD8+ T cell activation and cytolysis. Eur J Immunol 33, 3117–3126 (2003). [PubMed: 14579280]
50. Sata M, Walsh K, TNFalpha regulation of Fas ligand expression on the vascular endothelium modulates leukocyte extravasation. Nat Med 4, 415–420 (1998). [PubMed: 9546786]
51. Motz GT, Santoro SP, Wang LP, Garrabrant T, Lastra RR, Hagemann IS, Lal P, Feldman MD, Benencia F, Coukos G, Tumor endothelium FasL establishes a selective immune barrier promoting tolerance in tumors. Nat Med 20, 607–615 (2014). [PubMed: 24793239]
52. Lee WJ, Tateya S, Cheng AM, Rizzo-DeLeon N, Wang NF, Handa P, Wilson CL, Clowes AW, Sweet IR, Bomsztyk K, Schwartz MW, Kim F, M2 Macrophage Polarization Mediates Anti-inflammatory Effects of Endothelial Nitric Oxide Signaling. Diabetes 64, 2836–2846 (2015). [PubMed: 25845662]
53. Lu G, Zhang R, Geng S, Peng L, Jayaraman P, Chen C, Xu F, Yang J, Li Q, Zheng H, Shen K, Wang J, Liu X, Wang W, Zheng Z, Qi C-F, Si C, He JC, Liu K, Lira SA, Sikora AG, Li L, Xiong H, Myeloid cell-derived inducible nitric oxide synthase suppresses M1 macrophage polarization. Nature Communications 6, 1–14 (2015).
54. Lavin B, Gómez M, Pello OM, Castejon B, Piedras MJ, Saura M, Zaragoza C, Nitric oxide prevents aortic neointimal hyperplasia by controlling macrophage polarization. Arterioscler Thromb Vasc Biol 34, 1739–1746 (2014). [PubMed: 24925976]
55. Hou KK, Pan H, Lanza GM, Wickline SA, Melittin derived peptides for nanoparticle based siRNA transfection. Biomaterials 34, 3110–3119 (2013). [PubMed: 23380356]
56. Dunn GP, Bruce AT, Ikeda H, Old LJ, Schreiber RD, Cancer immunoediting: from immunosurveillance to tumor escape. Nat Immunol 3, 991–998 (2002). [PubMed: 12407406]

57. Dunn GP, Old LJ, Schreiber RD, The three Es of cancer immunoediting. Annu Rev Immunol 22, 329–360 (2004). [PubMed: 15032581]
58. Koebel CM, Vermi W, Swann JB, Zerafa N, Rodig SJ, Old LJ, Smyth MJ, Schreiber RD, Adaptive immunity maintains occult cancer in an equilibrium state. Nature 450, 903–907 (2007). [PubMed: 18026089]
59. Yin X, Grove L, Rogulski K, Prochownik EV, Myc target in myeloid cells-1, a novel c-Myc target, recapitulates multiple c-Myc phenotypes. J Biol Chem 277, 19998–20010 (2002). [PubMed: 11909865]
60. Qiu G, Xu Z, Huang D, Gong L, Li C, Sun X, Sun K, [Cloning and characterization of MTLC, a novel gene in 6q25]. Zhonghua yi xue yi chuan xue za zhi = Zhonghua yixue yichuanxue zazhi = Chinese journal of medical genetics 20, 94–97 (2003). [PubMed: 12673574]
61. Martin JD, Seano G, Jain RK, Normalizing Function of Tumor Vessels: Progress, Opportunities, and Challenges. Annu Rev Physiol 81, 505–534 (2019). [PubMed: 30742782]
62. Huang Y, Yuan J, Righi E, Kamoun WS, Ancukiewicz M, Nezivar J, Santosuosso M, Martin JD, Martin MR, Vianello F, Leblanc P, Munn LL, Huang P, Duda DG, Fukumura D, Jain RK, Poznansky MC, Vascular normalizing doses of antiangiogenic treatment reprogram the immunosuppressive tumor microenvironment and enhance immunotherapy. Proc Natl Acad Sci U S A 109, 17561–17566 (2012). [PubMed: 23045683]
63. Terme M, Pernot S, Marcheteau E, Sandoval F, Benhamouda N, Colussi O, Dubreuil O, Carpentier AF, Tartour E, Taieb J, VEGFA-VEGFR pathway blockade inhibits tumor-induced regulatory T-cell proliferation in colorectal cancer. Cancer Res 73, 539–549 (2013). [PubMed: 23108136]
64. Voron T, Colussi O, Marcheteau E, Pernot S, Nizard M, Pointet AL, Latreche S, Bergaya S, Benhamouda N, Tanchot C, Stockmann C, Combe P, Berger A, Zinzindohoue F, Yagita H, Tartour E, Taieb J, Terme M, VEGF-A modulates expression of inhibitory checkpoints on CD8+ T cells in tumors. J Exp Med 212, 139–148 (2015). [PubMed: 25601652]
65. Lai YS, Wahyuningtyas R, Aui SP, Chang KT, Autocrine VEGF signalling on M2 macrophages regulates PD-L1 expression for immunomodulation of T cells. Journal of cellular and molecular medicine 23, 1257–1267 (2019). [PubMed: 30456891]
66. Shitara K, Nishikawa H, Regulatory T cells: a potential target in cancer immunotherapy. Ann N Y Acad Sci 1417, 104–115 (2018). [PubMed: 29566262]
67. Munn LL, Jain RK, Vascular regulation of antitumor immunity. Science 365, 544–545 (2019). [PubMed: 31395771]
68. Johansson A, Hamzah J, Ganss R, More than a scaffold: Stromal modulation of tumor immunity. Biochim Biophys Acta 1865, 3–13 (2016). [PubMed: 26071879]
69. Fukumura D, Kloepper J, Amoozgar Z, Duda DG, Jain RK, Enhancing cancer immunotherapy using antiangiogenics: opportunities and challenges. Nat Rev Clin Oncol 15, 325–340 (2018). [PubMed: 29508855]
70. Tang Z, Kang B, Li C, Chen T, Zhang Z, GEPIA2: an enhanced web server for large-scale expression profiling and interactive analysis. Nucleic Acids Res 47, W556–w560 (2019). [PubMed: 31114875]
71. Brown CR, Reiner SL, Bone-marrow chimeras reveal hemopoietic and nonhemopoietic control of resistance to experimental Lyme arthritis. J Immunol 165, 1446–1452 (2000). [PubMed: 10903749]
72. Halabi CM, Broekelmann TJ, Lin M, Lee VS, Chu ML, Mecham RP, Fibulin-4 is essential for maintaining arterial wall integrity in conduit but not muscular arteries. Sci Adv 3, e1602532 (2017). [PubMed: 28508064]
73. Jin SW, Beis D, Mitchell T, Chen JN, Stainier DY, Cellular and molecular analyses of vascular tube and lumen formation in zebrafish. Development 132, 5199–5209 (2005). [PubMed: 16251212]
74. Eckfeldt CE, Mendenhall EM, Flynn CM, Wang TF, Pickart MA, Grindle SM, Ekker SC, Verfaillie CM, Functional analysis of human hematopoietic stem cell gene expression using zebrafish. PLoS Biol 3, e254 (2005). [PubMed: 16089502]
75. Guy CT, Cardiff RD, Muller WJ, Induction of mammary tumors by expression of polyomavirus middle T oncogene: a transgenic mouse model for metastatic disease. Mol Cell Biol 12, 954–961 (1992). [PubMed: 1312220]

76. Noguchi T, Ward JP, Gubin MM, Arthur CD, Lee SH, Hundal J, Selby MJ, Graziano RF, Mardis ER, Korman AJ, Schreiber RD, Temporally Distinct PD-L1 Expression by Tumor and Host Cells Contributes to Immune Escape. Cancer Immunol Res 5, 106–117 (2017). [PubMed: 28073774]

77. Timmins NE, Nielsen LK, Generation of multicellular tumor spheroids by the hanging-drop method. Methods Mol Med 140, 141–151 (2007). [PubMed: 18085207]

78. Nakatsu MN, Hughes CC, An optimized three-dimensional in vitro model for the analysis of angiogenesis. Methods Enzymol 443, 65–82 (2008). [PubMed: 18772011]

79. Steinritz D, Schmidt A, Balszuweit F, Thiermann H, Ibrahim M, Bolck B, Bloch W, Assessment of Endothelial Cell Migration After Exposure to Toxic Chemicals. J Vis Exp, e52768 (2015). [PubMed: 26274775]

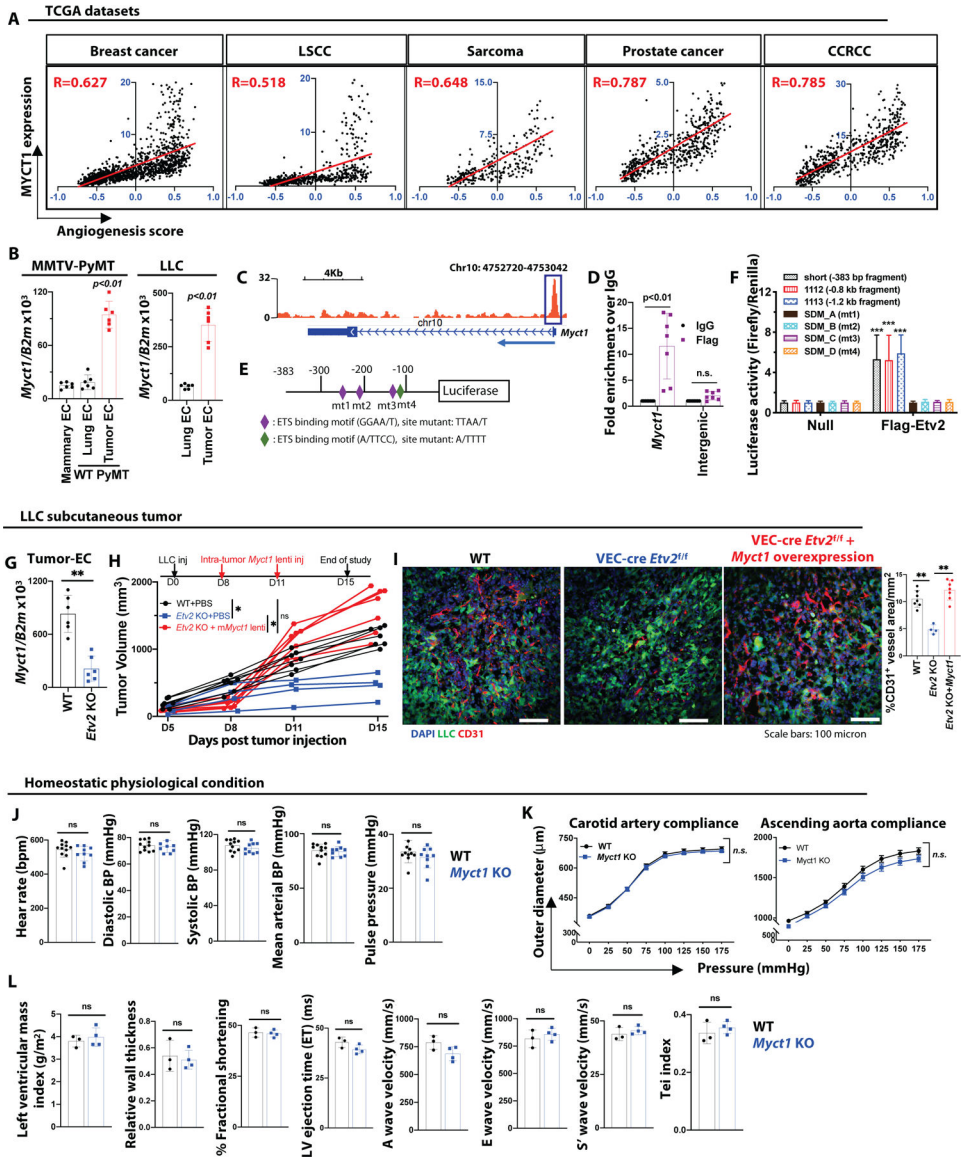

Figure 1: ETV2 direct target gene *Myct1* is a regulator of angiogenesis but is not required for vascular development and homeostasis.

(A) Correlation between the 'angiogenic score' and *MYCT1* expression in TCGA-derived breast cancer (TCGA-BRCA), LSCC (TCGA-LUSC), sarcoma (TCGA-SARC), prostate cancer (TCGA-PRAD), and CCRCC (TCGA-KIRC) patient datasets (Pearson's $\chi 2$ test; *R* values are indicated with respective datasets). (B) Analysis of *Myct1* expression in $CD31^{+}CD45^{-}$ ECs isolated from the mammary glands of healthy wild-type (WT) mice, and the lungs and mammary tumors of WT MMTV-PyMT mice at 21 weeks of age (left) and lungs and tumors of the tumor-bearing WT mice at 14-days post LLC tumor transplantation (right). n=6 mice per group. Data is presented as mean with standard deviation (SD) from one of two biological replicates. Statistical significance was analyzed by One-way ANOVA with Tukey's multiple comparison test (left) and two-tailed Student's t-test (right). (C) A genomic snapshot illustrating the ETV2 binding peak to the *Myct1* promoter region. (D) ChIP-qPCR analysis of ETV2 binding to the *Myct1* promoter region. Data is presented as

mean with SD. Statistical significance was analyzed by Two-way ANOVA followed by Tukey's multiple comparison test. mt=mutant. (E and F) A graphical representation of the luciferase construct design (E) and analysis of the normalized reporter activity (F) for ETV2 binding motif on *Myct1*. Data is presented as mean with SD. Statistical significance was analyzed by One-way ANOVA with Tukey's multiple comparison test; ***$p<0.001$, compared to the respective values in the absence of ETV2 (null). (G) Analysis of *Myct1* expression in $CD31^{+}CD45^{-}$ ECs isolated from the tumors of WT and *VEC-Cre;Etv2*$^{f/f}$ (*Etv2* KO)mice at 15-days post LLC tumor transplantation. n=6 mice per group. Data is presented as mean with SD from one of two biological replicates. Statistical significance was analyzed by two-tailed Student's t-test. (H and I) Tumor growth (H) and representative images with quantification for $CD31^{+}$ vessel density (I) in PBS (control) and *Myct1* lentiviral overexpression construct (intra-tumor) treated WT and *Etv2* KO mice. n=7 mice per group. Scale bars, 100μm. Data is presented as mean with SD from one of two biological replicates. Statistical significance was analyzed by two-tailed Student's t-test; *$p<0.05$, at the end of the study. (J and K) Analysis of vital cardiovascular parameters (J) and pressure-diameter measurements (K) in the *Myct1* KO and WT mice. n=9 (*Myct1* KO) and 11 (WT) mice. Data is presented as mean with SD from one of two biological replicates. Statistical significance was analyzed by two-tailed Student's t-test (J) and One-way ANOVA with Tukey's multiple comparison test (K); n.s.=not significant. (L) Analysis of clinically important cardiac functional parameters measured by Doppler echocardiogram of *Myct1* KO and WT mice. n=3 (WT) and 4 (*Myct1* KO) mice. Data is presented as mean with SD. Statistical significance was analyzed by two-tailed Student's t-test; n.s.=not significant.

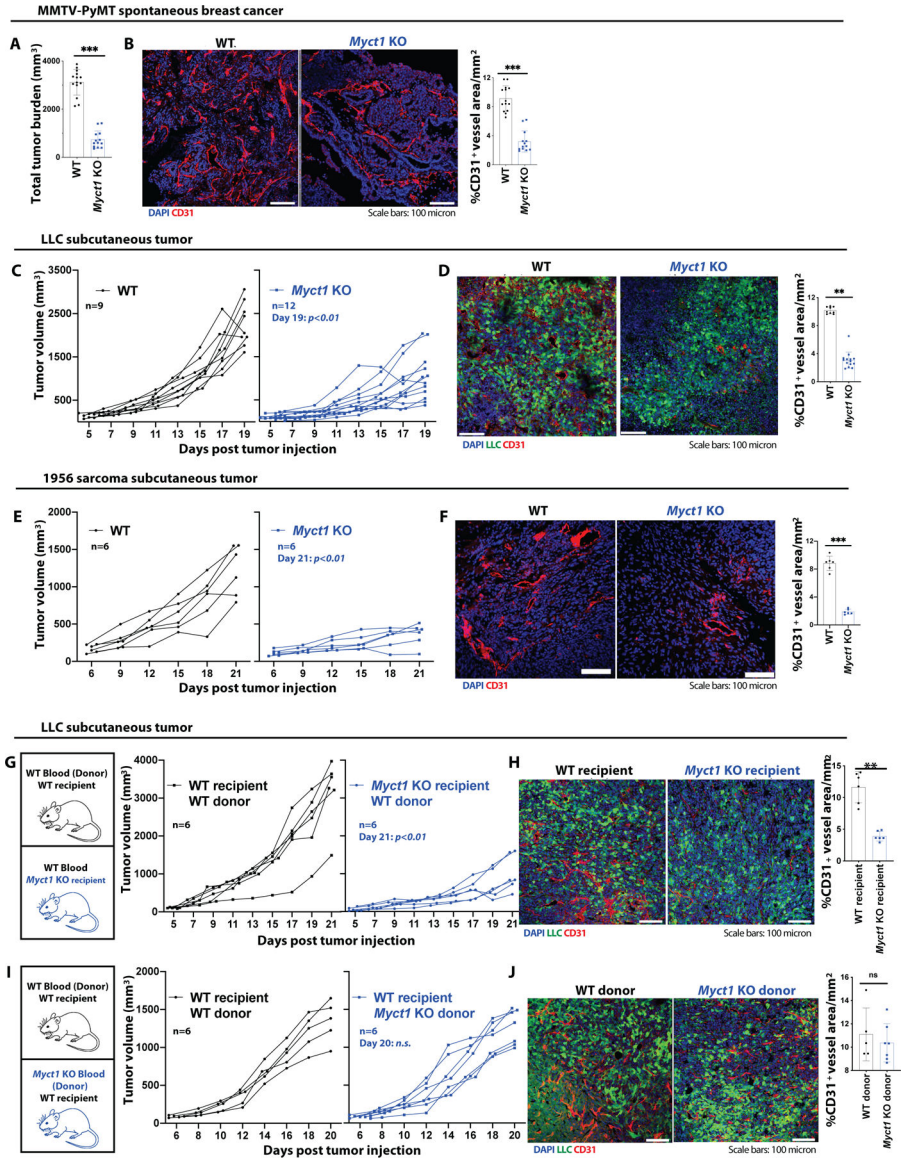

Figure 2: Endothelial *Myct1* is required for tumor growth and angiogenesis in mice.

(A and B) Analysis of total tumor burden (A) and representative images with quantification of CD31$^+$ vessel density (B) in WT and *Myct1* KO MMTV-PyMT mice at 21 weeks of age. n=14 mice per group. Scale bars, 100μm. Data is presented as mean with SD. Statistical significance was analyzed by two-tailed Student's t-test; ****p<0.001*. (C, D) Analysis of LLC tumor growth (C) and representative images with quantification for CD31$^+$ vessel density (D) in WT and *Myct1* KO mice. Scale bars, 100μm. Data is presented as mean with SD from one of three biological replicates. Statistical significance was analyzed by two-tailed Student's t-test; ***p<0.01*, at the end of the study. (E and F) Analysis of 1956-sarcoma tumor growth (E) and representative images with quantification for CD31$^+$ vessel density (F) in WT and *Myct1* KO mice. Scale bars, 100μm. Data is presented as mean with SD from one of three biological replicates. Statistical significance was analyzed by two-tailed Student's t-test; ***p<0.001*, at the end of the study. (G-J) Analysis of tumor growths (G and I) and

representative images with quantification for $CD31^+$ vessel density (H and J) in stromal *Myct1* KO (G and H) and hematopoietic *Myct1* KO mice (I and J). Scale bars, 100μm. Data is presented as mean with SD. Statistical significance was analyzed by two-tailed Student's t-test; n.s.=not significant and $**p<0.01$, at the end of the study.

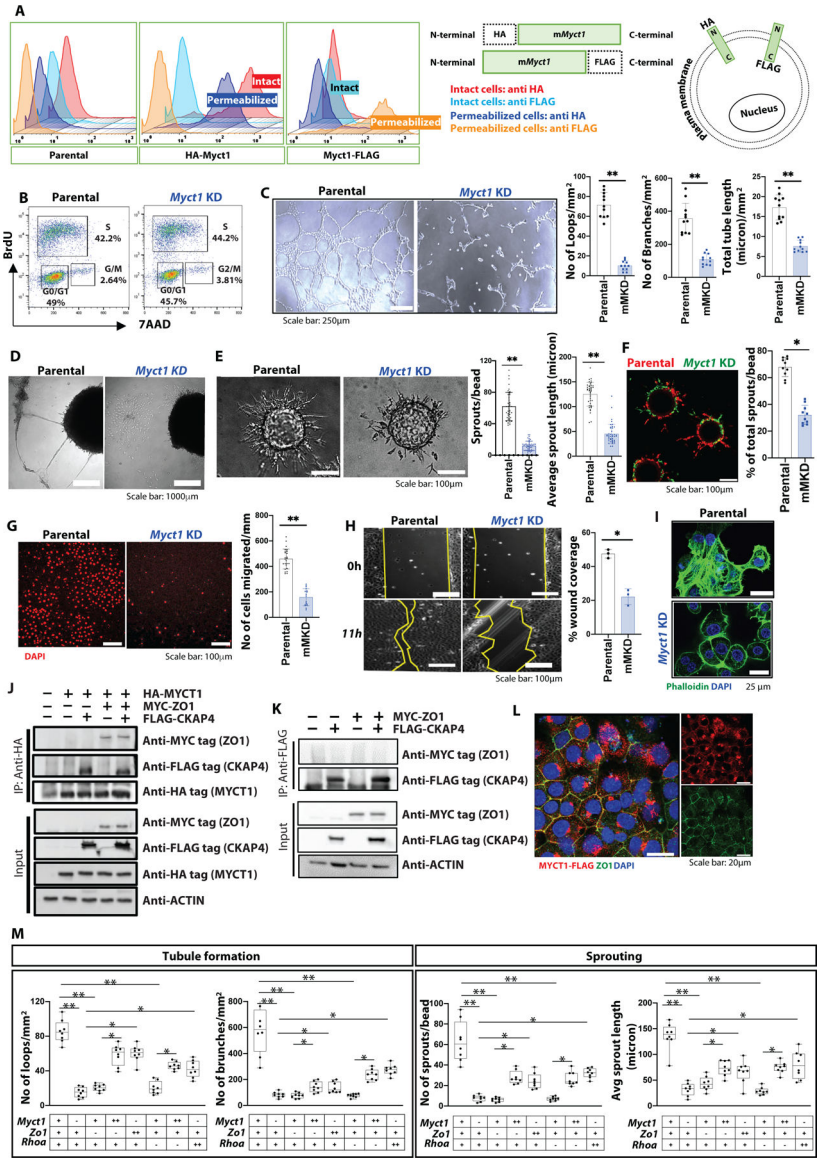

Figure 3: Membrane-localized MYCT1 regulates endothelial actin cytoskeleton dynamics in the angiogenic environment.

(A) (left) Flow cytometric analysis of HA- and FLAG-tagged MYCT1 overexpressing MCEC cells. (right) A graphical presentation of the HA- and FLAG-tagged MYCT1 protein situated at the plasma membrane. (B) A representative FACS chart of the BrdU proliferation assay with parental and *Myct1* knockdown (KD) cells. (C) Representative images and quantifications from the Matrigel tube formation assay. n=12 independent observations per group. Scale bars, 250μm. Data is presented as mean with SD from one of three biological replicates. Statistical significance was analyzed by two-tailed Student's t-test; ***p<0.01.* (D) Representative images from tumor-spheroid/EC co-culture assay. Scale bar, 1000μm. (E) Representative images and quantifications of sprouts from the fibrin gel sprouting assay. n≥32 independent observations per group. Scale bars, 100μm. Data is presented as mean with SD from one of three biological replicates. Statistical significance was analyzed by two-tailed Student's t-test; ***p<0.01.* (F) Representative image and quantification of sprouts

from the fibrin gel sprouting assay with 1:1 competitive seeding of parental (red) and *Myct1* KD (green) MCEC cells on the beads. Scale bar, 100μm. Data is presented as mean with SD. Statistical significance was analyzed by two-tailed Student's t-test; ***p<0.05*. (G) Representative images and quantifications of cell migration from the Boyden chamber assay. n≥12 independent observations per group. Scale bars, 100μm. Data is presented as mean with SD from one of three biological replicates. Statistical significance was analyzed by two-tailed Student's t-test; ***p<0.01*. (H) Representative images and quantifications for recovery from the wound closure assay. n≥3 independent observations per group. Scale bars, 100μm. Data is presented as mean with SD from one of two biological replicates. Statistical significance was analyzed by two-tailed Student's t-test; ***p<0.05*. (I) Representative immunofluorescence images of actin filaments in a cultured monolayer of MCEC cells. Scale bars, 25μm. (J) Immunoprecipitation followed by western blot (IP-WB) analysis for MYCT1 in the total cell lysates of the parental and HA-tagged MYCT1 overexpressing (HA-MYCT1) MCEC cells transfected with either mock (empty vector control) or MYC-tagged ZO1, and FLAG-tagged CKAP4 expression plasmids. An anti-ACTIN antibody was used as a control. (K) IP-WB analysis for CKAP4 in the total cell lysates of the parental MCEC cells transfected with either mock (empty vector control), or MYC-tagged ZO1, or FLAG-tagged CKAP4 expression plasmids. An anti-ACTIN antibody was used as a control. (L) Representative immunofluorescence image of ZO1 (green) and MYCT1 (anti-FLAG, red) in a confluent monolayer of FLAG-tagged MYCT1 overexpressing MCEC cells. Scale bars, 20μm. (M) Quantifications from the Matrigel tube formation assay (left) and fibrin gel sprouting assay (right) with different combinations of *Myct1*, *Zo1*, and *Rhoa* KD and overexpressing MCEC cells. "+", "++", and "−" denotes parental, overexpression, and knockdown cells, respectively. n≥6 independent observations per group. Data is presented as mean with SD from one of two biological replicates. Statistical significance was analyzed by One-way ANOVA with Tukey's multiple comparison test; **p<0.05, **p<0.01*.

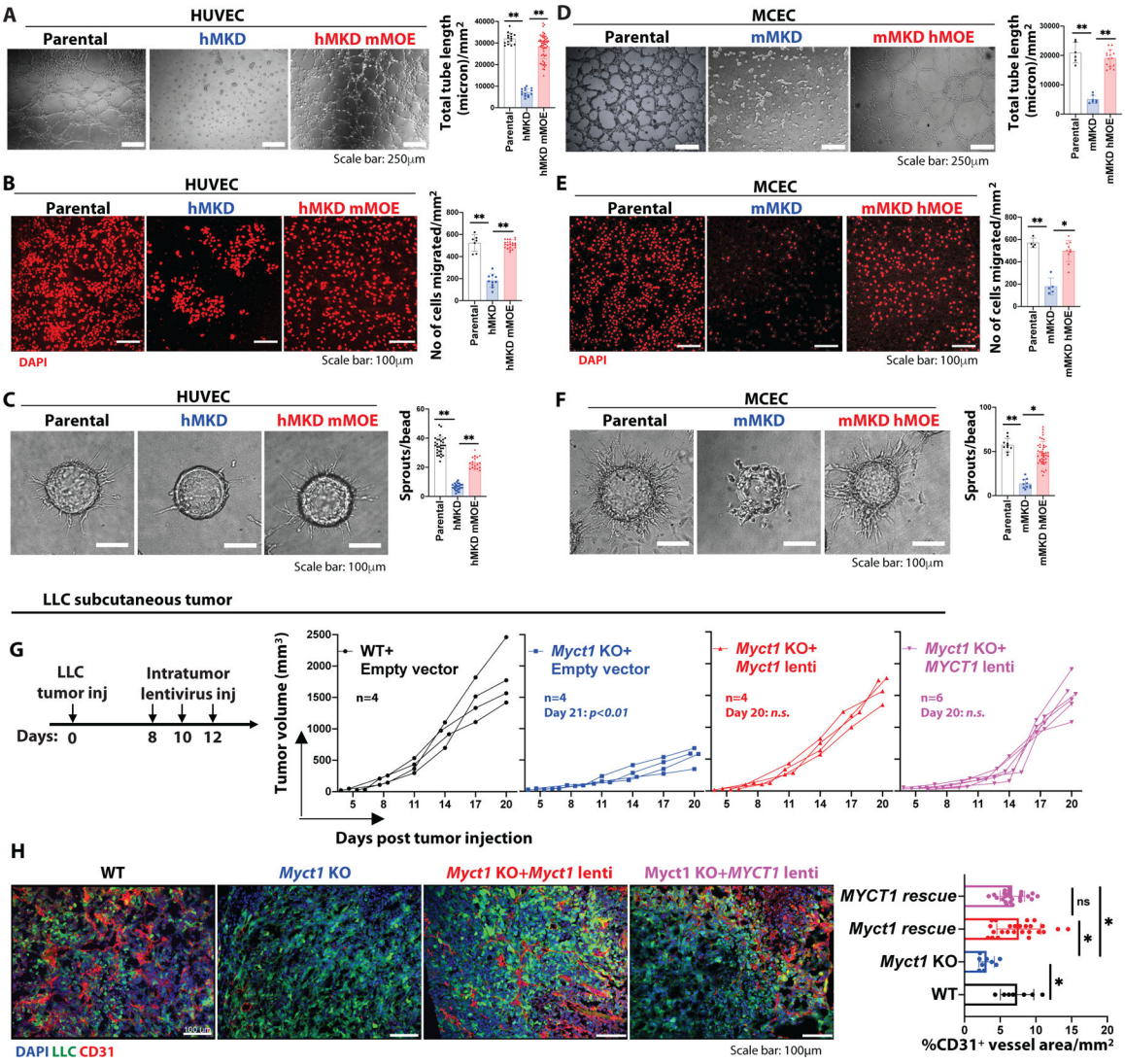

Figure 4: Endothelial MYCT1 function is evolutionarily conserved between human and mouse.

(A-C) Representative images and quantifications from the Matrigel tube formation assay (A), Boyden chamber migration assay (B), and fibrin gel bead sprouting angiogenesis assay (C) with parental, human *MYCT1* KD (hMKD), and mouse *Myct1* overexpressing human *MYCT1* KD (hMKD mMOE) HUVEC cells. Scale bar, 250μm (A) and 100μm (B and C). n≥10 independent observations per group. Data is presented as mean with SD from one of three biological replicates. Statistical significance was analyzed by One-way ANOVA with Tukey's multiple comparison test; ***p<0.05*. (D-F) Representative images and quantifications from the Matrigel tube formation assay (D), Boyden chamber migration assay (E), and fibrin gel sprouting assay (F) with parental, mouse *Myct1* KD (mMKD), and human *MYCT1* overexpressing mouse *Myct1* KD (mMKD hMOE) MCEC cells. Scale bars, 250μm (D) and 100μm (E and F). n≥10 independent observations per group. Data is presented as mean with SD from one of three biological replicates. Statistical significance was analyzed by One-way ANOVA with Tukey's multiple comparison test; **p<0.05* and ***p<0.01*. (G and H) Analysis of tumor growth (G) and representative immunofluorescence

images with quantification for $CD31^+$ vessel density (H) in PBS (control) and either mouse *Myct1* or human *MYCT1* lentiviral overexpression constructs (intra-tumor) treated WT and *Myct1* KO mice. Scale bars, 100μm. Data is presented as mean with SD. Statistical significance was analyzed by One-way ANOVA with Tukey's multiple comparison test; n.s.=not significant and $*p<0.05$, at the end of the study.

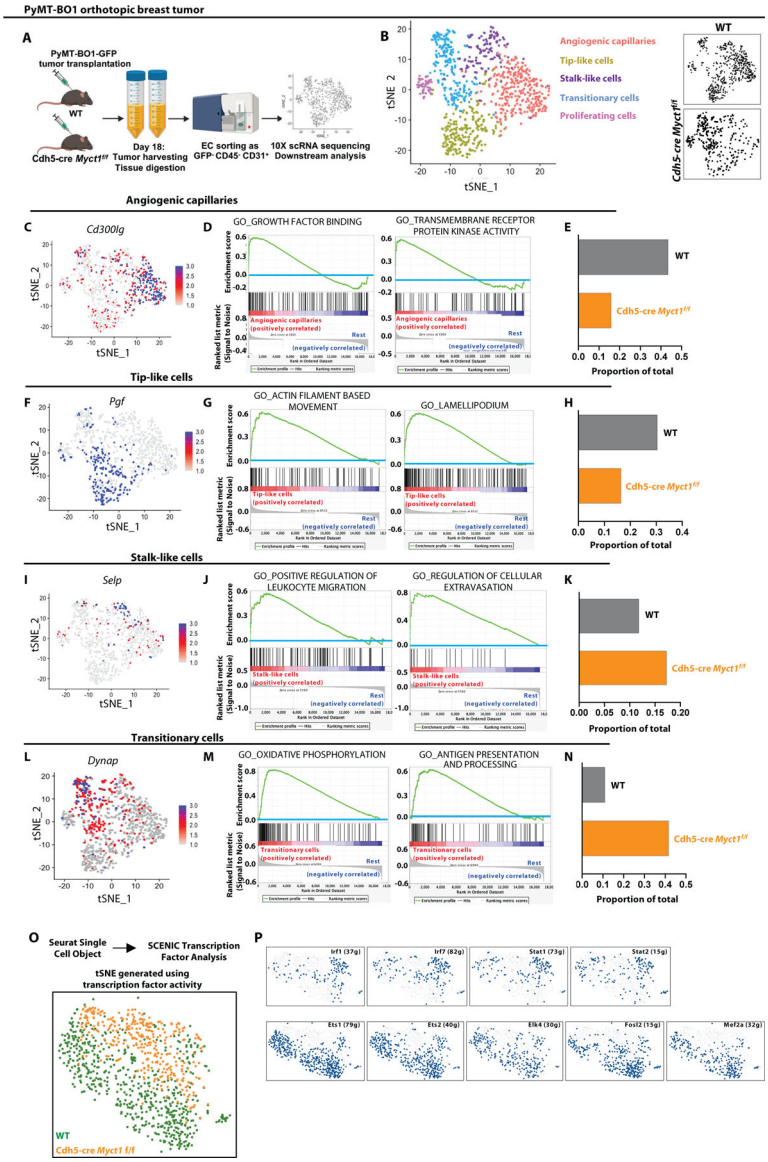

Figure 5: Single cell RNA sequencing of tumor endothelium from WT and Cdh5-cre *Myct1*$^{f/f}$ mice signifies *Myct1* functions in tumor angiogenesis.

(A) A schematic representation of tumor endothelium sample collection and processing from WT and Cdh5-cre *Myct1*$^{f/f}$ mice (n = 5 per group) for single cell RNA sequencing. (B) (Left) tSNE projection color-coded for 995 endothelial cells sorted from tumor mass (PYMT-BO1 orthotopic transplantation tumor model). (Right) tSNE projection of endothelial cells grouped for different genotypes. (C-E) Feature plot showing *Cd300lg* expression pattern (C), gene set enrichment analysis depicting enriched molecular pathways (D), and normalized proportion of cells (E) in the angiogenic capillaries sub-cluster of the tumor endothelial cells from WT and Cdh5-cre *Myct1*$^{f/f}$ mice derived by analyzing the SCTtransform data (normalized). (F-H) Feature plot showing *Pgf* expression pattern (F), gene set enrichment analysis depicting enriched molecular pathways (G), and normalized proportion of cells (H) in the Tip-like cells sub-cluster of the tumor endothelial cells from WT and Cdh5-cre *Myct1*$^{f/f}$ mice derived by analyzing the SCTtransform data (normalized).

(I-K) Feature plot showing *Selp* expression pattern (I), gene set enrichment analysis depicting enriched molecular pathways (J), and normalized proportion of cells (K) in the Stalk-like cells sub-cluster of the tumor endothelial cells from WT and Cdh5-cre $Myct1^{f/f}$ derived by analyzing the SCTtransform data (normalized). (L-N) Feature plot showing *Dynap* expression pattern (L), gene set enrichment analysis depicting enriched molecular pathways (M), and normalized proportion of cells (N) in the Transitionary cells sub-cluster of the tumor endothelial cells from WT and Cdh5-cre $Myct1^{f/f}$ derived by analyzing the SCTtransform data (normalized). (O and P) tSNE projection (O) and area under the curve (AUC) plots for differentially enriched transcription factor activity modules (P) in WT and Cdh5-cre $Myct1^{f/f}$ tumor endothelium generated by using SCENIC analysis.

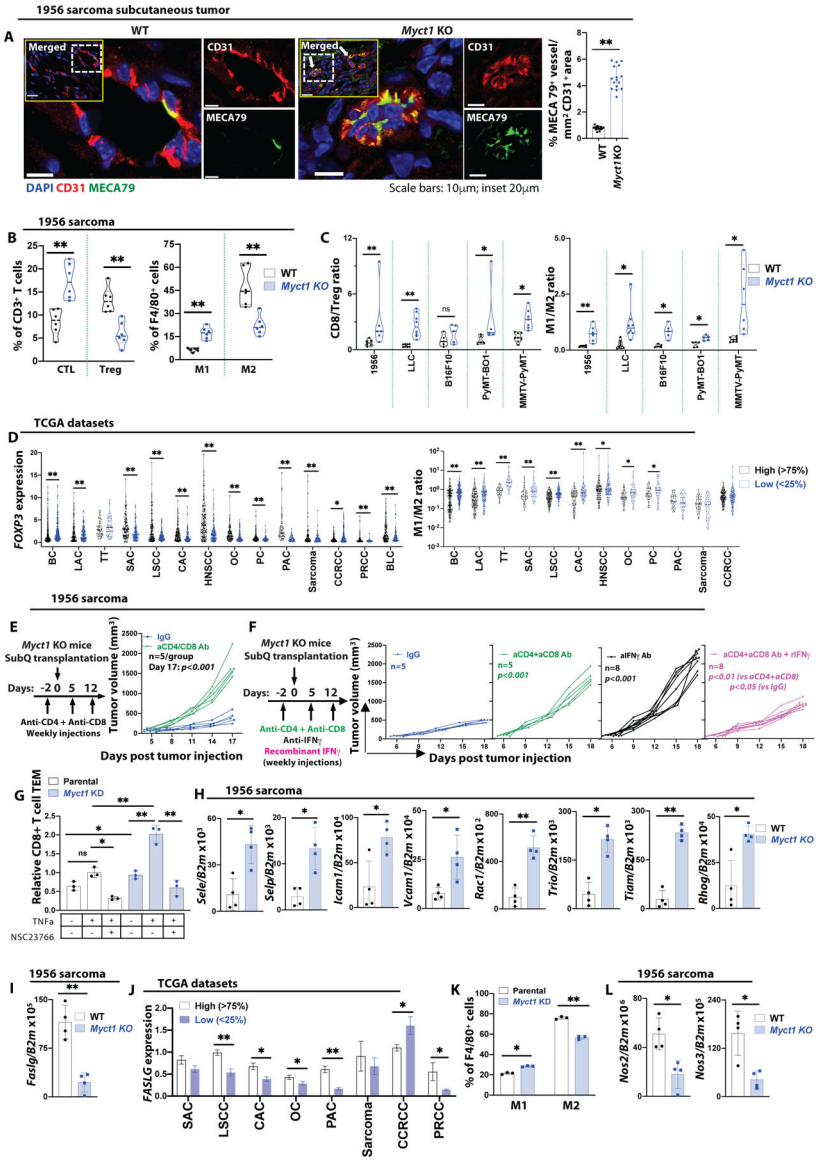

Figure 6: *Myct1* deficiency promotes an immunostimulatory tumor microenvironment.

(A) Representative immunofluorescence images and quantification of MECA79$^+$ high endothelial venules (HEVs) in 1956 sarcoma tumor. White dotted boxed area from the inset is presented as zoomed-in. Arrows in the inset indicate the MECA79 expressing vessels. Scale bars, 10μm and 20μm (inset). Data is presented as mean with SD. Statistical significance was analyzed by two-tailed Student's t-test; ***p<0.01*. (B) CTL (CD8$^+$ T cells) and Treg (CD4$^+$FOXP3$^+$ T cells) cells as a percentage of CD3$^+$ T cells and M1 (iNOS$^+$ macrophages) and M2 (CD206$^+$ macrophage) populations as a percentage of F4/80$^+$ cells. n=6 mice per group. Data is presented as mean with SD. Statistical significance was analyzed by two-tailed Student's t-test; ***p<0.01*. (C) Analysis of CD8/Treg and M1/M2 ratios as measures of immunosuppression in the tumor microenvironment of WT and *Myct1* KO mice. n=6 mice per group. Data is presented as mean with SD. Statistical significance was analyzed by two-tailed Student's t-test; n.s.=not significant, **p<0.05*, and ***p<0.01*. (D)

(top) Analysis of *FOXP3* expression in high vs. low *MYCT1* expressing tumors in patients from the TCGA database. (bottom) Analysis of M1/M2 population ratios in high vs. low *MYCT1* expressing tumors obtained by analyzing the TCGA patient datasets with the CIBERSORT algorithm. Datasets utilized were BC (TCGA-BRCA), LAC (TCGA-LUAD), TT (TCGA-TGCT), SAC (TCGA-STAD), LSCC (TCGA-LUSC), CAC (TCGA-COAD), HNSCC (TCGA-HNSC), OC (TCGA-OV), PC (TCGA-PRAD), PAC (TCGA-PDAC), Sarcoma (TCGA-SARC), CCRCC (TCGA-KIRC), PRCC (TCGA-KIRP), and BLC (TCGA-BLCA). Data is presented as scatter plot with the mean value. Statistical significance was analyzed by Mann-Whitney U test; *$p<0.05$ and **$p<0.01$ (E) Analysis of tumor growth in either IgG or combined anti-CD4 and anti-CD8 neutralizing antibody treated *Myct1* KO mice. n=5 mice per group. Data is presented as mean with SD from one of two biological replicates. Statistical significance was analyzed by One-way ANOVA with Tukey's multiple comparison test; $p<0.001$, at the end of the study. (F) Analysis of tumor growth in either IgG, or anti-IFNγ neutralizing antibody, or combined anti-CD4 and anti-CD8 neutralizing antibody, or combined anti-CD4 and anti-CD8 neutralizing antibody with IFNγ cytokine treated *Myct1* KO mice. Data is presented as mean with SD. Statistical significance was analyzed by One-way ANOVA with Tukey's multiple comparison test; '*p*-values' indicated on the figure are calculated at the end of the study. (G) Transendothelial migration (TEM) of $CD8^+$ T cells through parental and *Myct1* KD MCEC cell barrier with TNFα and Rac1 inhibitor NSC23766 pre-treatment. Data is presented as mean with SD. Statistical significance was analyzed by One-way ANOVA with Tukey's multiple comparison test; n.s.=not significant, *$p<0.05$, and **$p<0.01$. (H and I) Analysis of mRNA expression of the indicated genes in $CD31^+CD45^-$ ECs isolated from the 1956 sarcoma tumors. n=4 mice per group. Statistical significance was analyzed by Statistical significance was analyzed by two-tailed Student's t-test; *$p<0.05$ and **$p<0.01$. (J) *FASLG* expression profile in high vs. low *MYCT1* expressing tumors in SAC (TCGA-STAD), LSCC (TCGA-LUSC), CAC (TCGA-COAD), OC (TCGA-OV), PC (TCGA-PRAD), PAC (TCGA-PDAC), Sarcoma (TCGA-SARC), CCRCC (TCGA-KIRC), and PRCC (TCGA-KIRP) patients from the TCGA database. Data is presented as mean with standard error of mean. Statistical significance was analyzed by two-tailed Student's t-test; *$p<0.05$ and **$p<0.01$. (K) Polarization of peripheral blood-derived monocytes to M1 or M2 phenotype with LPS +IFNγ or IL4 cytokine treatment, respectively, in a coculture assay with either parental or *Myct1* KD MCEC cells, expressed as a percentage of F4/80+ macrophage population. Data is presented as mean with SD. Statistical significance was analyzed by two-tailed Student's t-test; *$p<0.05$ and **$p<0.01$. (L) Analysis of *Nos2* and *Nos3* mRNA expression in $CD31^+CD45^-$ ECs isolated from the 1956 sarcoma tumor. n=4 mice per group. Data is presented as mean with SD. Statistical significance was analyzed by two-tailed Student's t-test; **$p<0.01$.

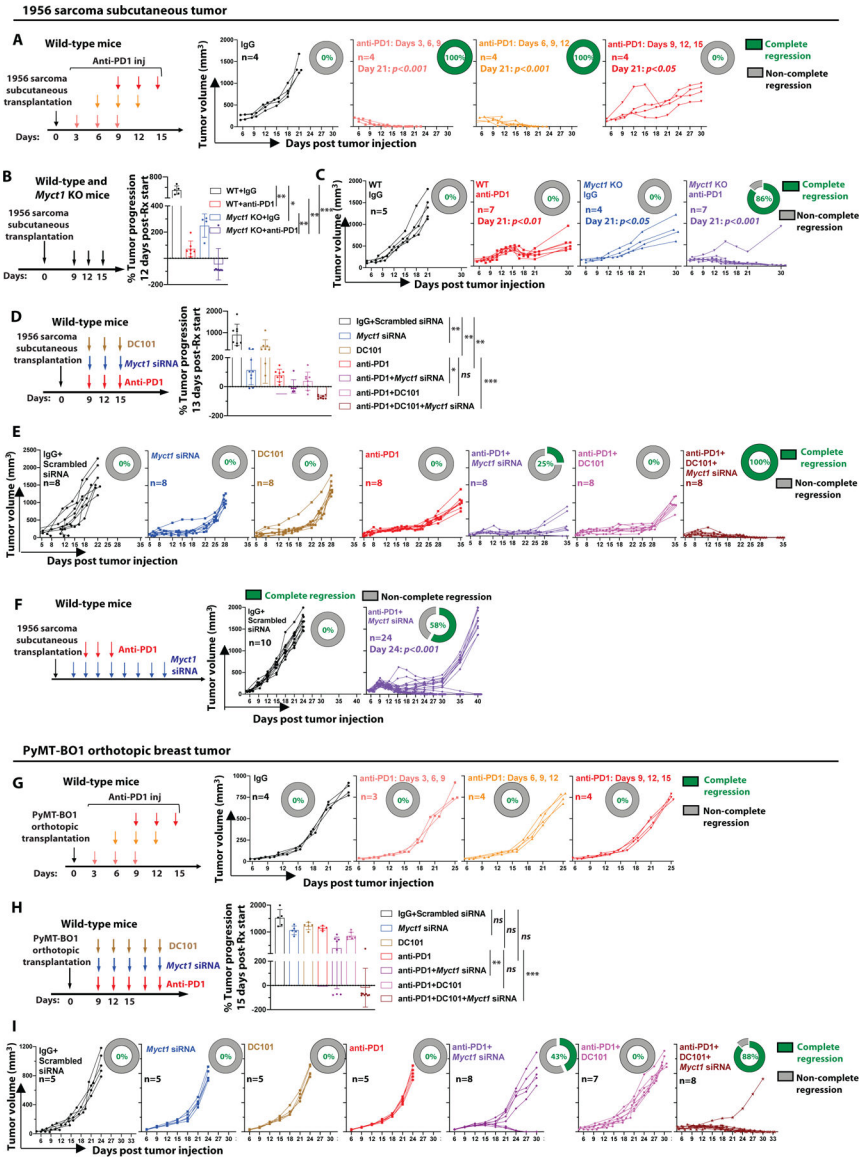

Figure 7: *Myct1*-targeted siRNA-peptide nanoparticle co-treatment improves anti-PD1 immunotherapy.

(A) Kinetics of tumor growth in 1956 sarcoma tumor bearing WT mice treated with anti-PD1 antibody in different indicated schemes. Donut charts display the percentage of subjects underwent complete regression (green) and non-complete regression (gray). Day-21 statistical significance was analyzed by One-way ANOVA with Tukey's multiple comparison test. (B) Analysis of tumor progression in 1956 sarcoma tumor bearing WT and *Myct1* KO mice at 12-days after anti-PD1 treatment initiation. Data is presented as mean with SD. Statistical significance was analyzed by One-way ANOVA with Tukey's multiple comparison test; $*p<0.05$, $**p<0.01$, and $***p<0.001$. (C) Tumor growth in 1956 sarcoma tumor bearing WT and *Myct1* KO mice treated with the anti-PD1 antibody. Donut charts display the percentage of subjects underwent complete regression (green) and non-complete regression (gray). Day-21 statistical significance was analyzed by One-way ANOVA with Tukey's multiple comparison test. (D) Analysis of tumor progression in 1956 sarcoma tumor

bearing WT mice at 13-days after treatment initiation as indicated. Data is presented as mean with SD. Statistical significance was analyzed by One-way ANOVA with Tukey's multiple comparison test; *$p<0.05$, **$p<0.01$, and ***$p<0.001$. (E) Tumor growth in 1956 sarcoma tumor bearing WT mice with different treatments as indicated. Donut charts display the percentage of subjects underwent complete regression (green) and non-complete regression (gray). (F) Tumor growth in 1956 tumor bearing WT mice treated with the anti-PD1 antibody in combination with an extended anti-*Myct1* siRNA-peptide nanoparticle treatment. Day-21 statistical significance was analyzed by One-way ANOVA with Tukey's multiple comparison test. (G) Kinetics of tumor growth in PyMT-BO1 tumor bearing WT mice treated with anti-PD1 antibody in different schemes. Donut charts display the percentage of subjects underwent complete regression (green) and non-complete regression (gray). (H) Tumor progression in PyMT-BO1 tumor bearing WT mice at 15-days after treatment initiation as indicated. Data is presented as mean with SD. Statistical significance was analyzed by One-way ANOVA with Tukey's multiple comparison test; n.s.=not significant, **$p<0.01$, and ***$p<0.001$. (I) Tumor growth in PyMT-BO1 tumor bearing WT mice with different treatments as indicated. Donut charts display the percentage of subjects underwent complete regression (green) and non-complete regression (gray).

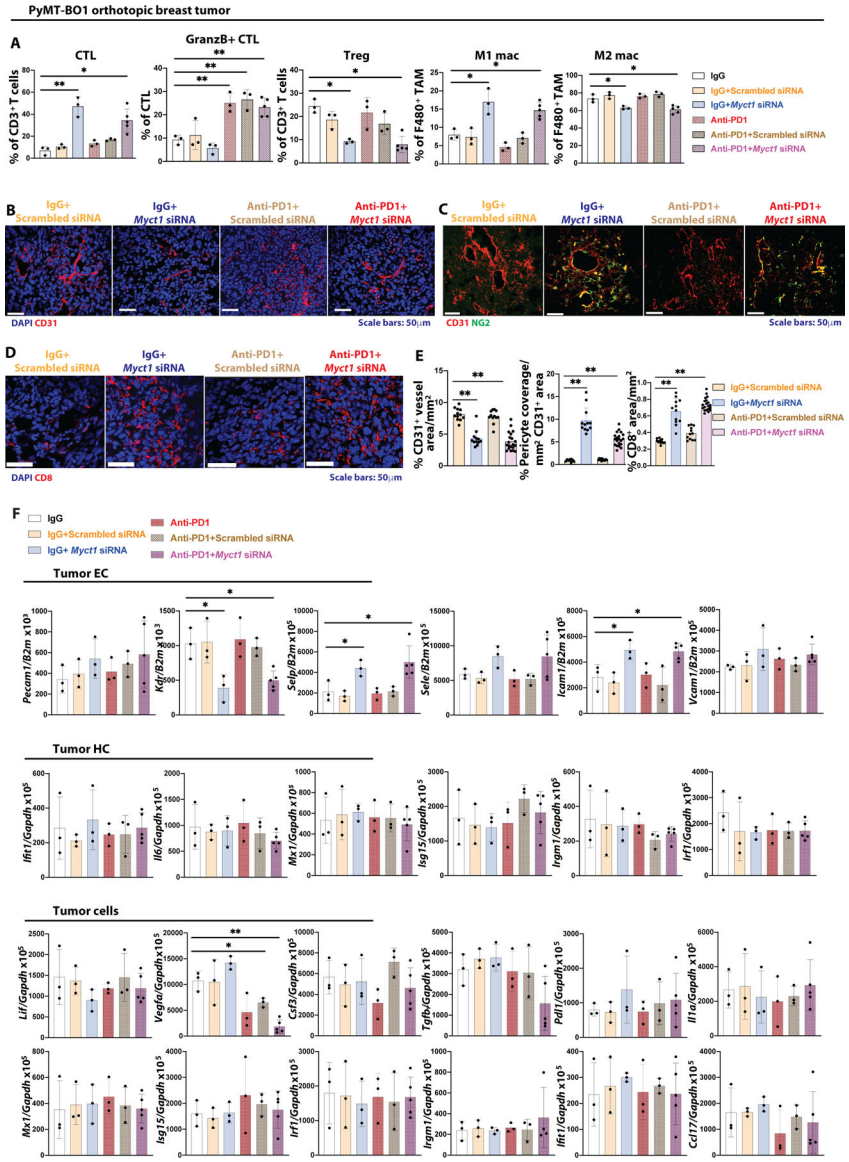

Figure 8: Anti-*Myct1* works synergistically with anti-PD1 treatment to improve outcomes in mice.

(A) Analysis of CTL ($CD8^+$ T cells) and Treg ($CD4^+FOXP3^+$ T cells) cells as a percentage of $CD3^+$ T cells, GranzB+ CTL as % of CTL cells, M1 ($iNOS^+$ macrophages) and M2 ($CD206^+$ macrophage) populations as a percentage of $F4/80^+$ cells in the tumor of the PyMT-BO1 tumor bearing WT mice with different combination of treatments as indicated. n=3–6 mice per group. Data is presented as mean with SD. Statistical significance was analyzed by One-way ANOVA with Tukey's multiple comparison test; *$*p<0.05$* and *$**p<0.01$*. (B-E) Representative images (B-D) and quantifications (E) for $CD31^+$ vascular density (B), pericyte coverage (C), and CD8+ T cell infiltration in the tumor mass of PyMT-BO1 tumor bearing WT mice with different combination of treatments as indicated. n=3–6 mice per group. Data is presented as mean with SD. Statistical significance was analyzed by One-way ANOVA with Tukey's multiple comparison test; *$**p<0.01$*. (F) Analysis of the expression of the indicated genes in the tumor ECs, hematopoietic cells (HC), and tumor

cells sorted from the PyMT-BO1 tumor bearing WT mice with different combination of treatments as indicated. n=3–6/group. Data is presented as mean with SD. Statistical significance was analyzed by One-way ANOVA with Tukey's multiple comparison test; *$p<0.05$ and **$p<0.01$.

Table 1.

Top 20 regulators of angiogenesis identified by their correlated expression with seed genes

Rank	Gene Symbol	Full name	PCC
1	*GPR4*	G Protein-Coupled Receptor 4	0.92
2	*LDB2*	LIM Domain Binding 2	0.91
3	*CXorf36*	Chromosome X open reading frame 36	0.91
4	*ADGRL4*	Adhesion G Protein-Coupled Receptor L4	0.91
5	*FLT1*	Fms Related Tyrosine Kinase 1	0.9
6	*CLEC14A*	C-Type Lectin Domain Containing 14A	0.9
7	*ECSCR*	Endothelial Cell Surface Expressed Chemotaxis and Apoptosis Regulator	0.9
8	*RP11–389C8.2*	*RP11–389C8.2*	0.9
9	*ESAM*	Endothelial Cell Adhesion Molecule	0.9
10	*MYCT1*	Myc Target 1	0.9
11	*CD93*	Cluster of Differentiation 93	0.9
12	*PLVAP*	Plasmalemma Vesicle Associated Protein	0.89
13	*S1PR1*	Sphingosine-1-Phosphate Receptor 1	0.89
14	*PTPRB*	Protein Tyrosine Phosphatase Receptor Type B	0.89
15	*ARHGEF15*	Rho Guanine Nucleotide Exchange Factor 15	0.89
16	*GIMAP8*	GTPase, IMAP Family Member 8	0.89
17	*PCDH12*	Protocadherin 12	0.88
18	*EXOC3L2*	Exocyst complex component 3-like 2	0.88
19	*ZNF366*	Zinc Finger Protein 366	0.88
20	*GIMAP6*	GTPase, IMAP Family Member 6	0.88

See also Supplementary Table 1. PCC = Pearson correlation coefficient